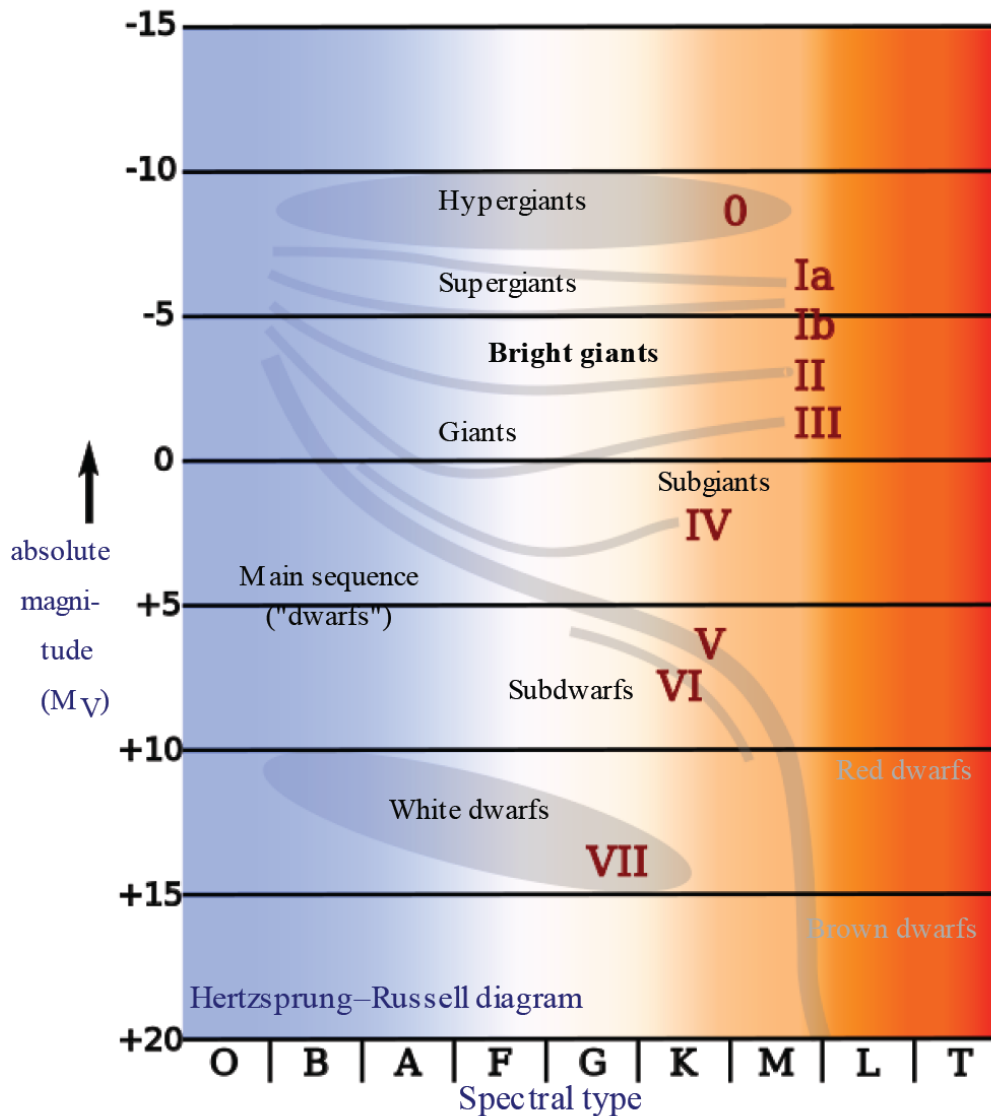


Post-main Sequence Evolution



Hypergiants

luminosity class 0; excessive mass loss

Supergiants

Ia luminous supergiants;
Ib supergiants; $Ia^+ = 0$

Subgiants

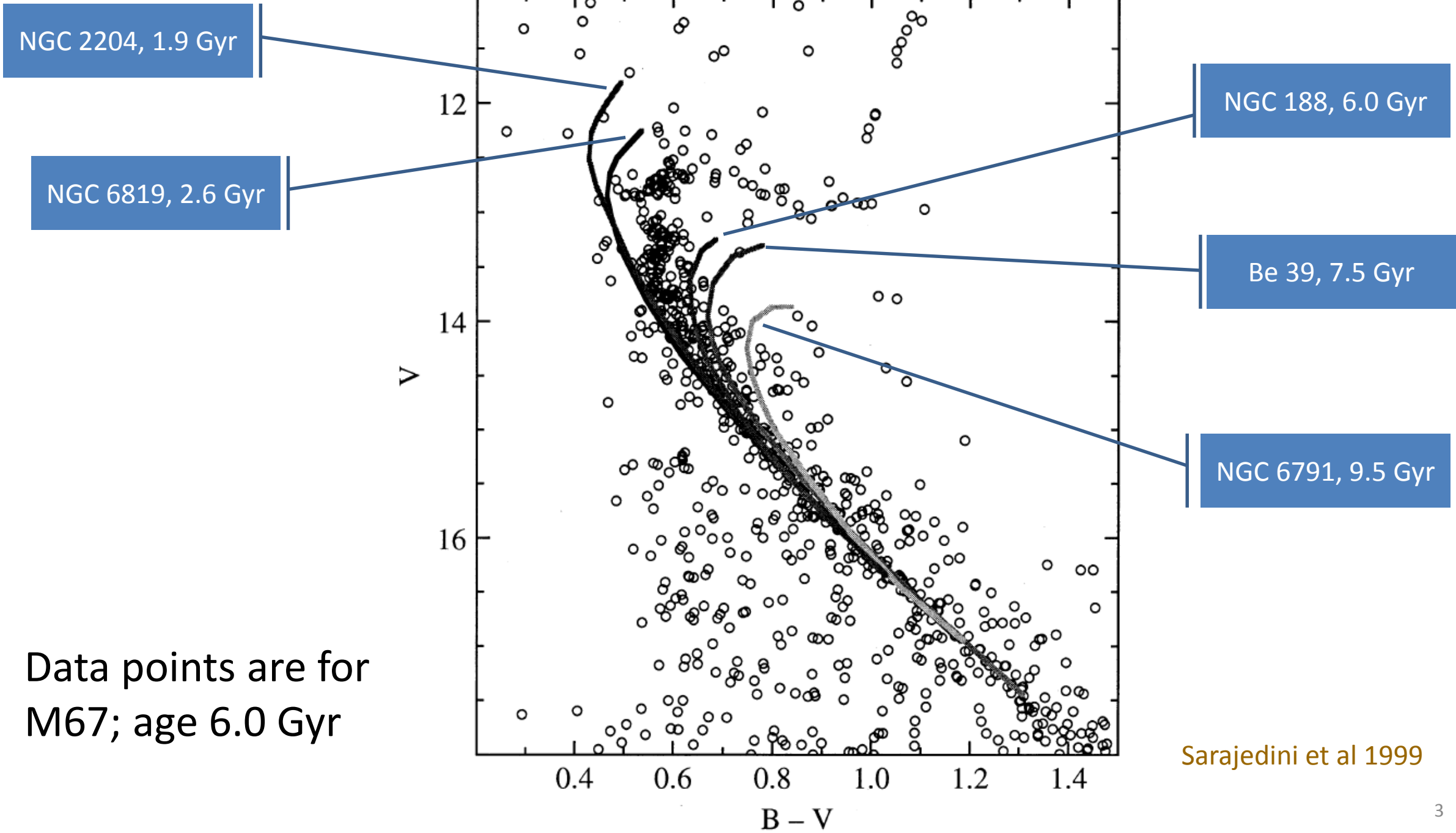
luminous class IV; between MS turn-off and the red giant branch

Dwarfs

luminosity class V = MS stars

Subdwarfs (sd)

luminosity class VI, 1.5 to 2 mag lower than MS; lower metallicity



NGC 2204, 1.9 Gyr

NGC 6819, 2.6 Gyr

NGC 188, 6.0 Gyr

Be 39, 7.5 Gyr

NGC 6791, 9.5 Gyr

Data points are for
M67; age 6.0 Gyr

Sarajedini et al 1999

Mass Loss during Stellar Evolution

- Stars lose mass at all evolutionary stages.
- Pre-main sequence: protostellar (bipolar) outflows
YSO jets, (star/disk) winds
- Main sequence: solar wind $\dot{\mathcal{M}} = 10^{-14} M_{\odot} \text{ yr}^{-1}$
For $\tau_{\text{MS}} \approx 10^{10} \text{ yr} \rightarrow \tau_{\text{loss,MS}} \approx 10^{-4} M_{\odot}$
Some stars, e.g., WR stars $\dot{\mathcal{M}} = 10^{-5} M_{\odot} \text{ yr}^{-1}$
- Post-main sequence: $R \uparrow \rightarrow g \downarrow$, and $P_{\text{rad}} \uparrow \Rightarrow \dot{\mathcal{M}} \uparrow$

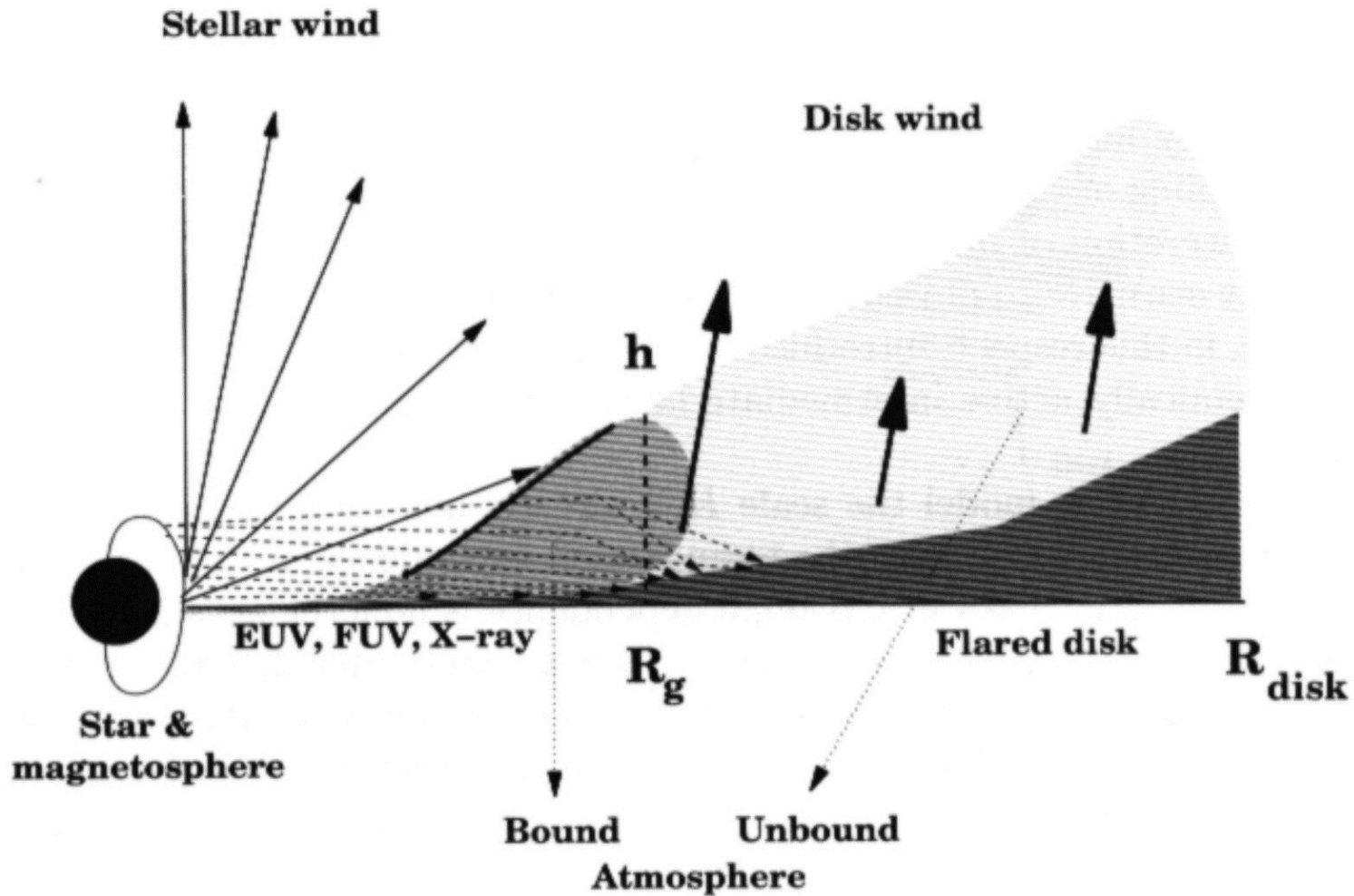


Fig. 7.6. Schematic representation of an irradiated flared disk. Below the radius R_g where matter remains bound by the gravity of the central star an optically thin atmosphere develops. Above this radius flared matter may escape and form some kind of slow wind. Adapted from Hollenbach et al. [403].

- For a stationary, isotropic wind, the mass loss rate

$$\dot{\mathcal{M}} = 4 \pi r^2 \rho(r) \frac{dr}{dt} = 4 \pi r^2 \rho(r) v(r) \quad v(r): \text{velocity law}$$

- $v(r) \uparrow$, at $r \rightarrow \infty$, $v_\infty \equiv v(r \rightarrow \infty)$ **terminal velocity**

Often $v(r) \approx v_0 + (v_\infty - v_0) \left(1 - \frac{R_*}{r}\right)^\beta$, where

$v_0 = v(R_*)$ at photosphere

- $\beta \leq 1$, $v \rightarrow v_\infty$ gradually $\beta \geq 1$, $v \rightarrow v_\infty$ slowly
- For hot stars, $\beta \approx 0.8$. Cool stars experience slower acceleration, so have larger β .

$$\dot{\mathcal{M}} = 4 \pi r^2 \rho(r) v(r) \quad \text{mass conservation}$$

$$\ddot{r} = -\frac{1}{\rho} \frac{dP}{dr} - \frac{GM}{r^2} = \frac{dv}{dt} = \frac{dv}{dr} \frac{dr}{dt} = v \frac{dv}{dr} \quad \text{momentum conservation}$$

Massive stars \rightarrow radiation pressure \rightarrow outer atmosphere expands supersonically \rightarrow winds driven by spectral-line opacity in UV.

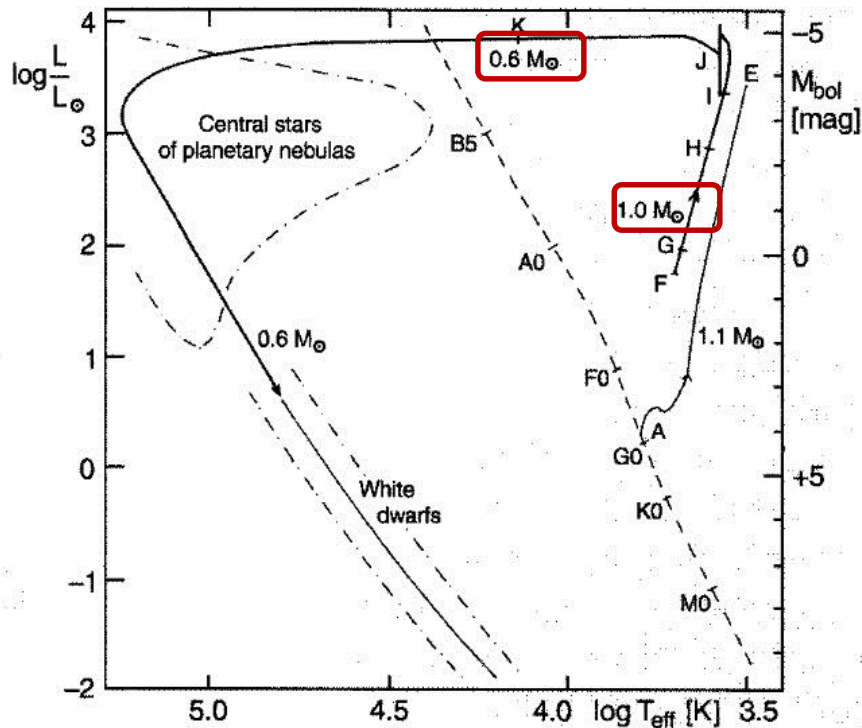


Fig. 8.8. The evolutionary paths in the Hertzsprung–Russell diagram of Population I stars having $1.0 M_{\odot}$ and $1.1 M_{\odot}$, from central hydrogen burning (A) to the helium flash (E), without taking mass losses into account. After A. V. Sweigart and P. G. Gross (1978). The ejection of a mass of $0.1 M_{\odot}$ during the helium flash was assumed. The further evolution of the star of $1.0 M_{\odot}$ was calculated taking the mass loss according to (7.105) into account, after D. Schönberner (1979). F \rightarrow G: the asymptotic giant branch; only one of the thermal pulses (helium flashes) which occur after I is drawn in, at J. The mass loss becomes important at H and leads to a final mass of $0.6 M_{\odot}$, which is reached at K

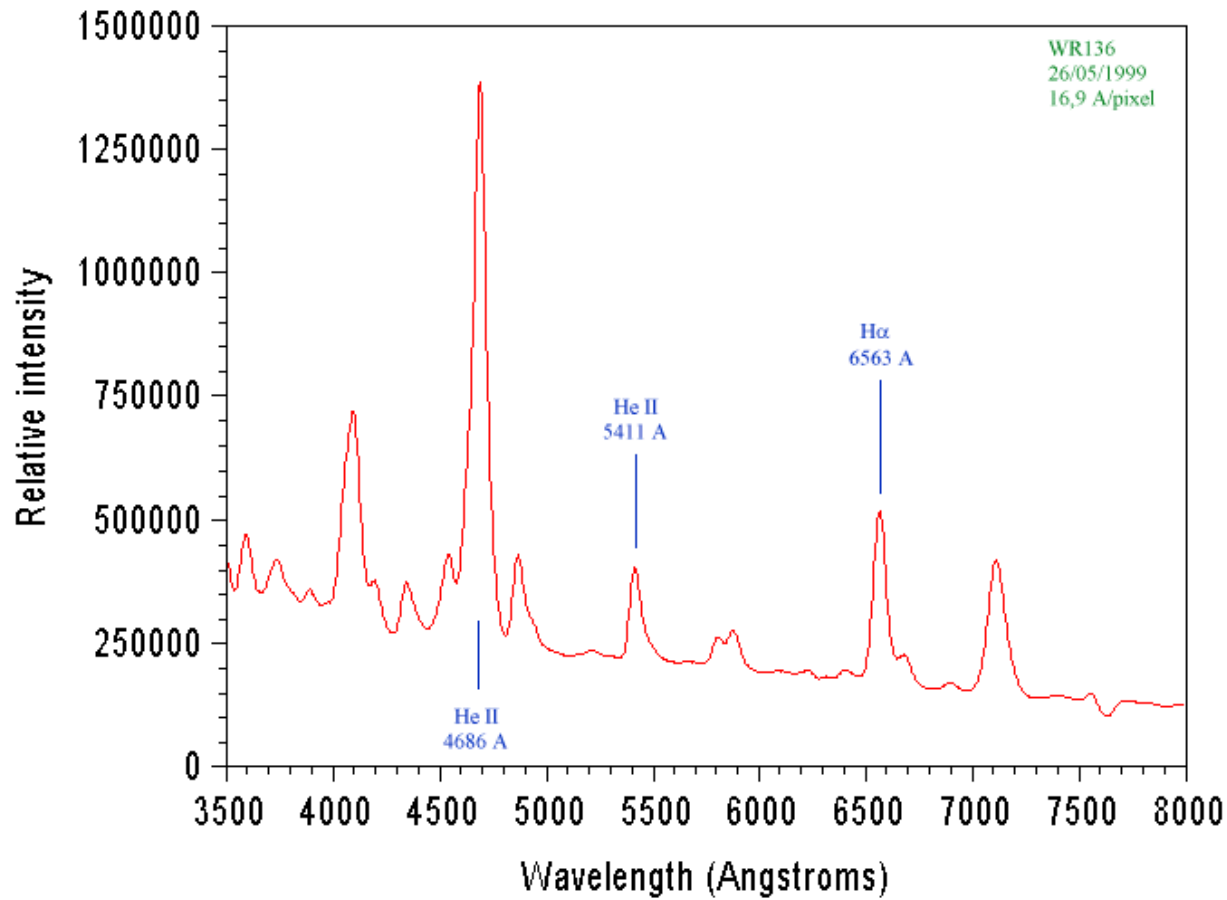
Mass loss (Reimers 1975)

$$\dot{M} \approx 4 \times 10^{-13} \frac{L/L_{\odot}}{(g/g_{\odot}) (R/R_{\odot})} [M_{\odot} \text{ yr}^{-1}]$$

$$g = GM/R^2$$

$$\text{Sun now } \dot{M} \approx 2 \times 10^{-14} M_{\odot} \text{ yr}^{-1}$$

$$\text{Cool supergiant } \dot{M} \approx 10^{-7} \text{ to } 10^{-5} M_{\odot} \text{ yr}^{-1}$$



WR stars

$T_{\text{eff}} \sim 25,000 \text{ to } 50,000 \text{ K}$

Evolved massive ($\geq 20 M_{\odot}$) stars

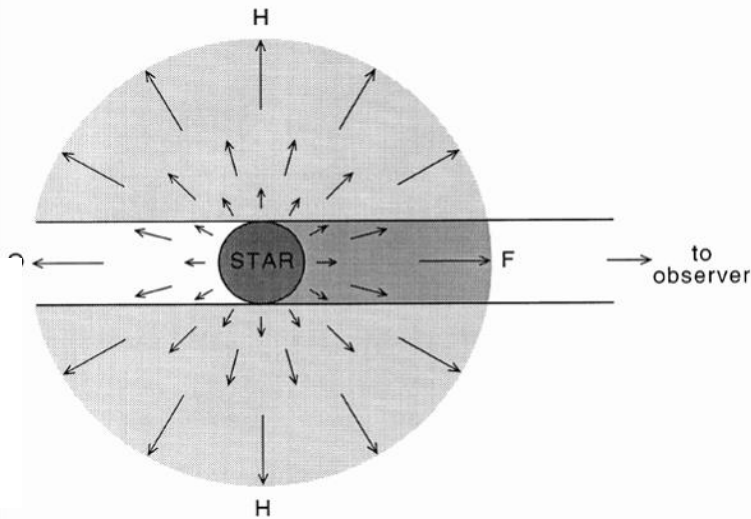
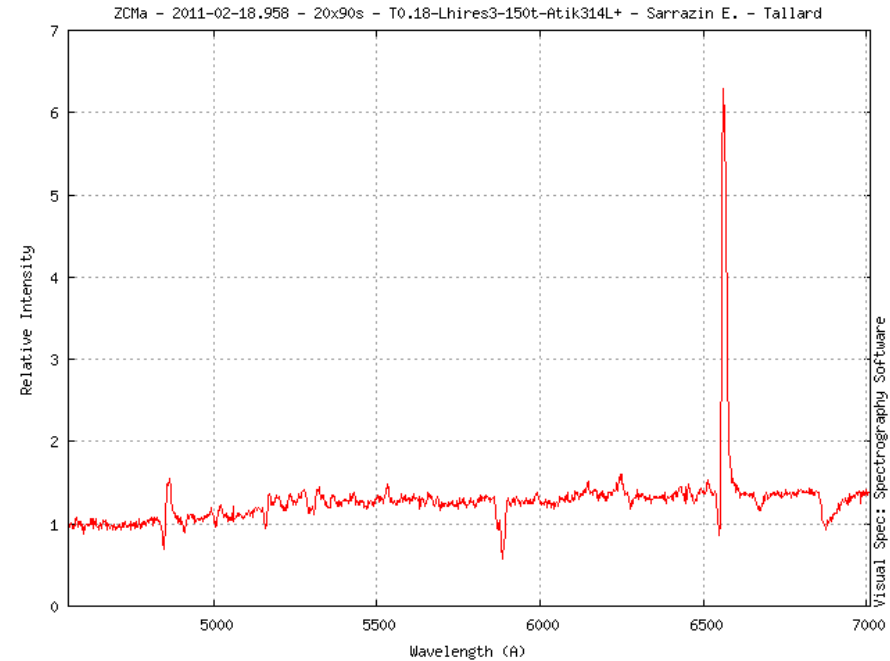
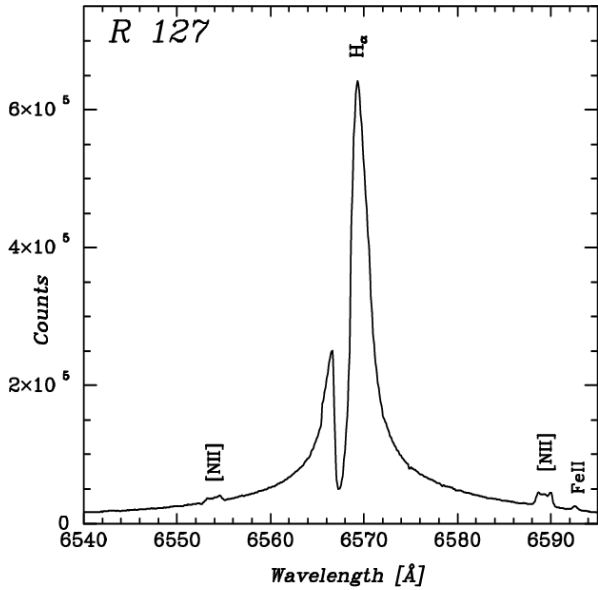
Wind $\sim 2000 \text{ km s}^{-1}$

$\dot{m} \sim 10^{-5} M_{\odot} \text{ yr}^{-1}$

Spectrum of a Wolf-Rayet star

$O(\rightarrow WN) \rightarrow LBV \rightarrow \begin{matrix} WN \\ WC \end{matrix}$

$\rightarrow \text{SNI}_{b,c}$



P Cygni profile of a spectral line
 --- a blue-shifted absorption
 superimposed on an emission line
 → **mass loss** (cool gas toward us)

P Cygni stars

- **Higher mass-loss rate, $> 10^{-5} M_{\odot} \text{ yr}^{-1}$**
- **Lower terminal velocity, $v_{\infty} < 10^{2.5} \text{ km s}^{-1}$**
- **Higher wind density, $n_H > 10^{10} \text{ cm}^{-3}$ at $2 R_*$**

than normal stars (Lamers 1986).

Stellar Pulsation

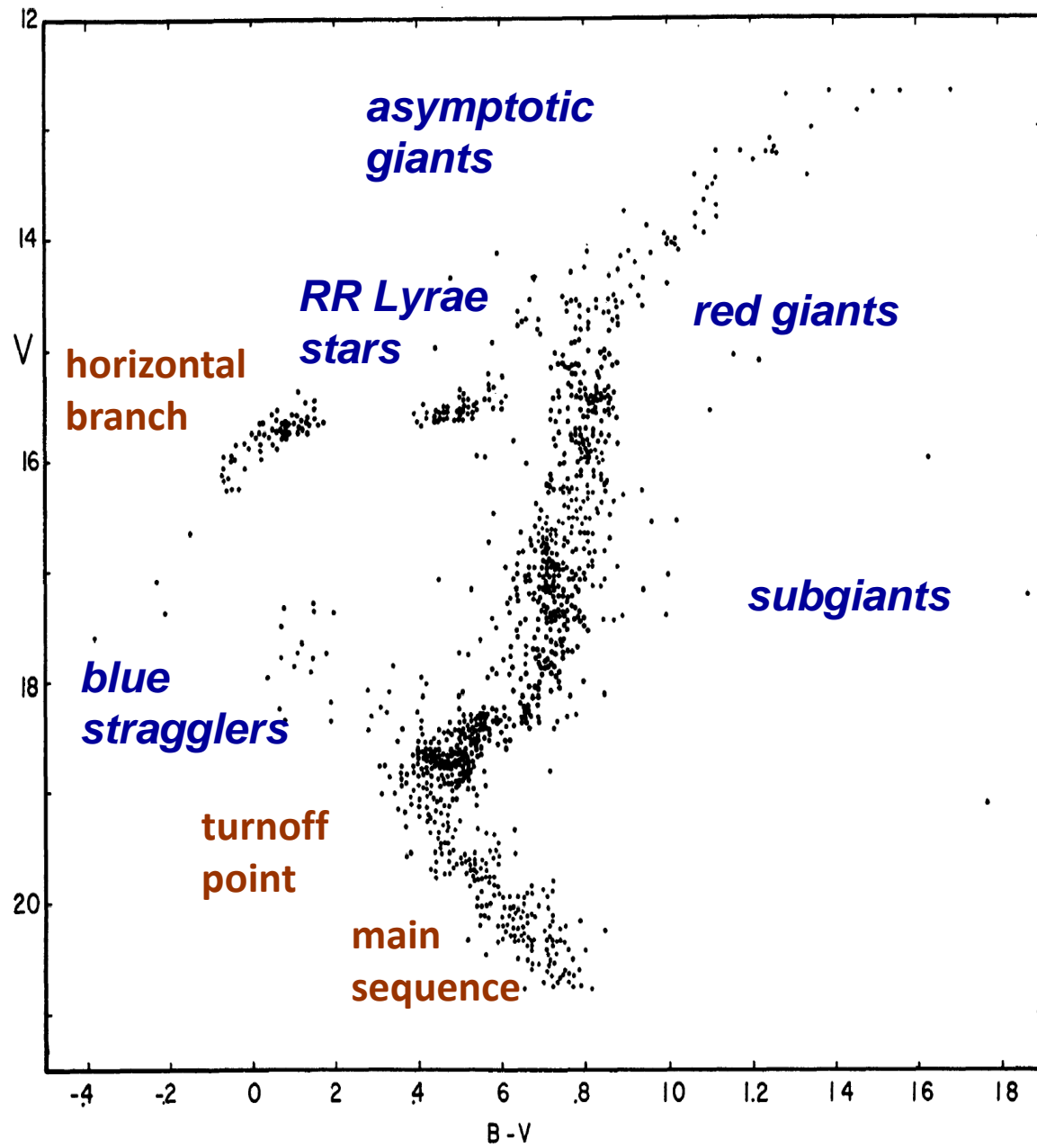
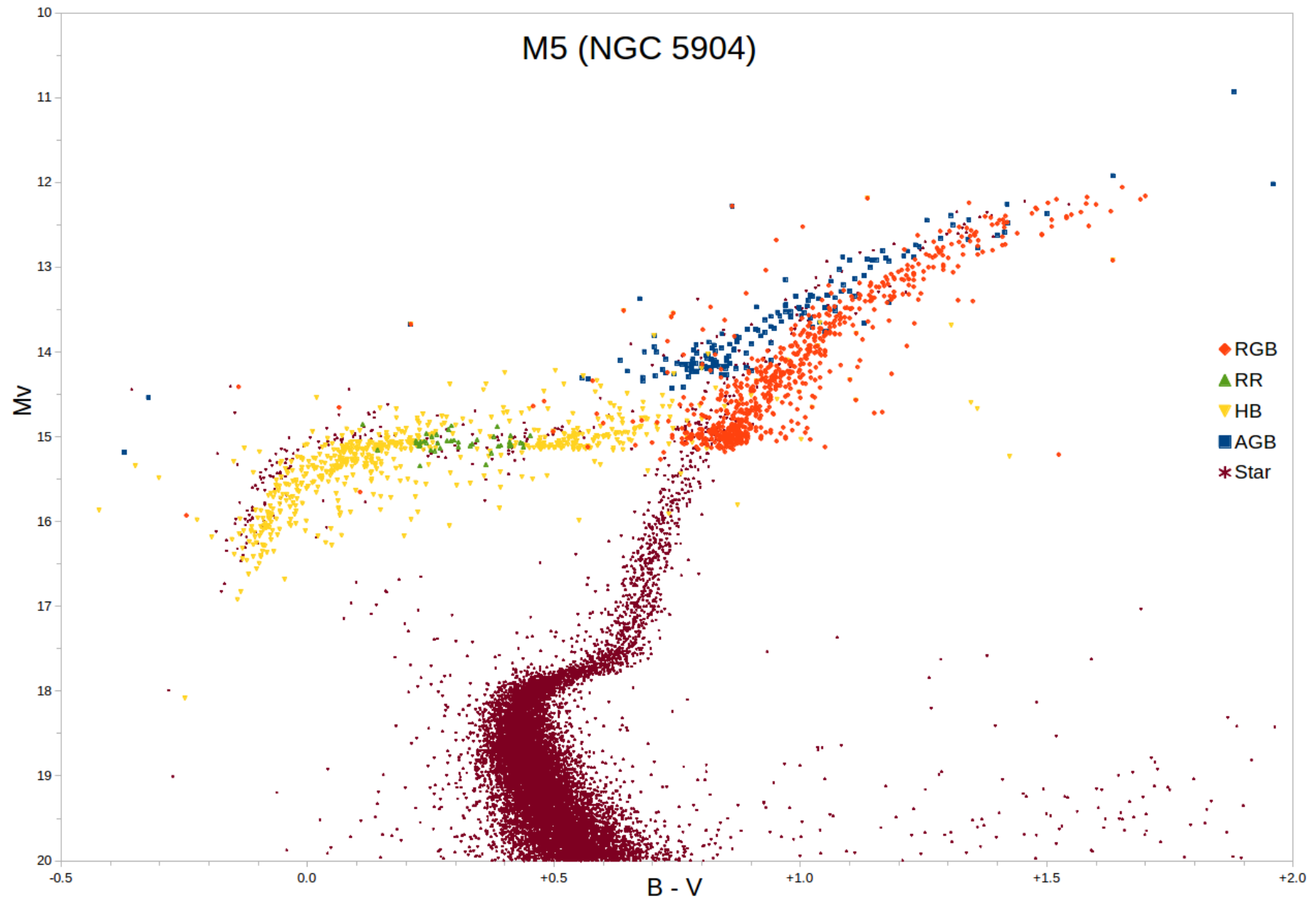


FIG. 5.—Color-magnitude diagram for M3 stars in the arguments V and $B - V$



https://en.wikipedia.org/wiki/Subgiant#/media/File:M5_colour_magnitude_diagram.png

Stellar Variability

- Time to transmit a perturbation of pressure changes across the star

$$t_{\text{vib}} \sim \frac{2R}{\bar{v}_s} \quad \text{where} \quad v_s = \sqrt{\gamma \frac{P_g}{\rho}}$$

$\gamma = c_p/c_V = 5/3$ for monatomic gas.

- Virial theorem, $2K + \Omega = 0, \therefore v_s^2 = \frac{GM}{R}$

$$t_{\text{vib}} \sim \frac{2R}{\sqrt{GM/R}} \sim \frac{1}{\sqrt{G\rho}}$$

cf. free-fall time

Approximate Relation between Stellar Density, Pulsation and Minimum Rotational Period

Star	Density g cm^{-3}	t_{vib} sec	$t_{\text{rot, min}}$ sec
Neutron star	10^{15}	10^{-4}	3×10^{-4}
White Dwarf	10^7	1	3
RR Lyrae star	10^{-2}	$10^{4.5}$	10^5
Cepheid Variable	10^{-6}	$10^{6.5}$	10^7

t (Crab Nebula) ~ 33 ms \rightarrow cannot be a white dwarf

- ❖ **Rotational Variation** --- sub-seconds .. weeks
- ❖ **Pulsational Variation** --- hours .. weeks
- ❖ **Orbital (Eclipsing Binaries)** --- hours .. days

Valve mechanism (Eddington)

• Heating $\rightarrow P \uparrow \rightarrow$ expansion \rightarrow cooling

\therefore Self-regulated stability

• Absorption of radiation

• Usually $\kappa \propto T^{-n}$

\therefore Heating $\rightarrow T \uparrow \rightarrow \kappa \downarrow \rightarrow$ cooling

• contraction \rightarrow releases energy

expansion \rightarrow absorbs energy

Normally $T \nearrow \rightarrow \kappa \searrow$

Recall Kramers opacity

κ mechanism — a partially ionized layer
to absorb energy during compression
(and release energy during expansion)

In stars, there are 2 ionization zones

— $T \sim (1-1.5) \times 10^4$ K hydrogen ionization zone
 $H I \rightarrow H II$, $He I \rightarrow He II$

— $T \sim (4-5) \times 10^4$ K
 $He II \rightarrow He III$
helium ionization zone

But if there is an ionization layer,
e.g., $He^+ \rightarrow He^{++}$

$T \nearrow \rightarrow \kappa \nearrow$
energy trapped
 \rightarrow expansion

Energy escaped
 \rightarrow Contraction

\rightarrow pulsation

Depths of ionization zones

e.g. $T_{\text{eff}} \gtrsim 7500 \text{ K}$, zones near surface

→ not enough mass available to drive the oscillation.

$T_{\text{eff}} \gtrsim 5500 \text{ K}$, zones deeper

⇒ significant pulsation

$T_{\text{eff}} < 5500 \text{ K}$, convective outer layer

→ pulsation suppresses

∴ $T_{\text{eff}} \sim 5500 - 7500 \text{ K}$ for pulsation to take place, Instability "strip"

There is a certain surface temperature range for stellar pulsation ...

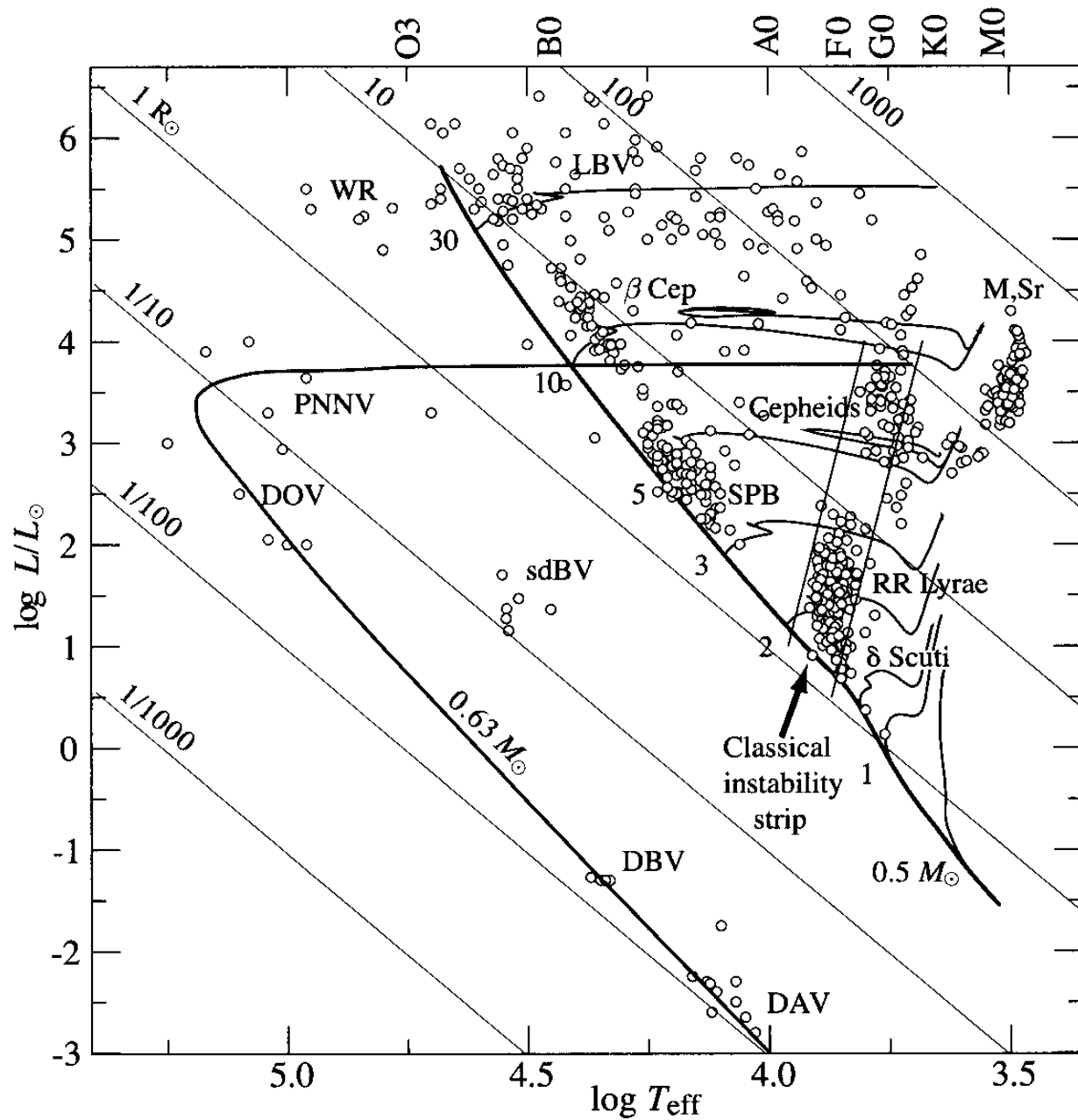


Figure 4.9. Examples of various types of pulsating variable stars plotted as small circles on the Hertzsprung–Russell diagram. The dark line to the right is the main sequence with evolutionary tracks branching off to the right for different stellar masses. The ultimate evolutionary track of a star that ends its life as a compact star of $0.63 M_{\odot}$ is shown. It moves leftward through the planetary nebulae nuclei variables (PNNV) and then downward as a cooling white dwarf, passing through regions of pulsational instability sequentially classified as DOV, DBV, and DAV (DAV = Dwarf + type/temperature A + Variable). Other types of intrinsic variables are shown: β Cephei stars, Mira (M), Semiregular (Sr), luminous blue (LBV), Wolf–Rayet (WR), slowly pulsating B stars (SPB), and subdwarf B stars (sdBV). The *classical instability strip* is shown as two parallel lines encompassing Cepheid, RR Lyrae, and δ Scuti variables; if extended, it intersects the pulsating DAV stars. The thin lines represent loci of constant radius. [Provided by A. Gautschy; see Gautschy H. Saio, *ARAA* 33, 77 (1995)]

Bradt “Astrophysics Processes”

Normally, $T \uparrow \Rightarrow K \downarrow$

plays a role also in red giants

Core \rightarrow increased energy output

Envelope \rightarrow expansion, cooling $\rightarrow K \uparrow$

\Rightarrow Red giants have convective envelopes.

cf PMS Hayashi tracks

The envelope extends from just outside of the H-burning shell to the surface.

\rightarrow 'Dredge-up' of processed material
from deep interior to surface

e.g., observations of heavy elements or
isotope ratios in evolved stars different
from (enrichment) young stars
(in a star cluster)

⇒ Evidence of stellar evolution
.. of nuclear reactions.

Convection \rightarrow chemical mixing

Much more efficient than the slow change of chemical composition produced by nuclear reaction.

In a convection region, $\frac{\partial X_i}{\partial m} = 0$

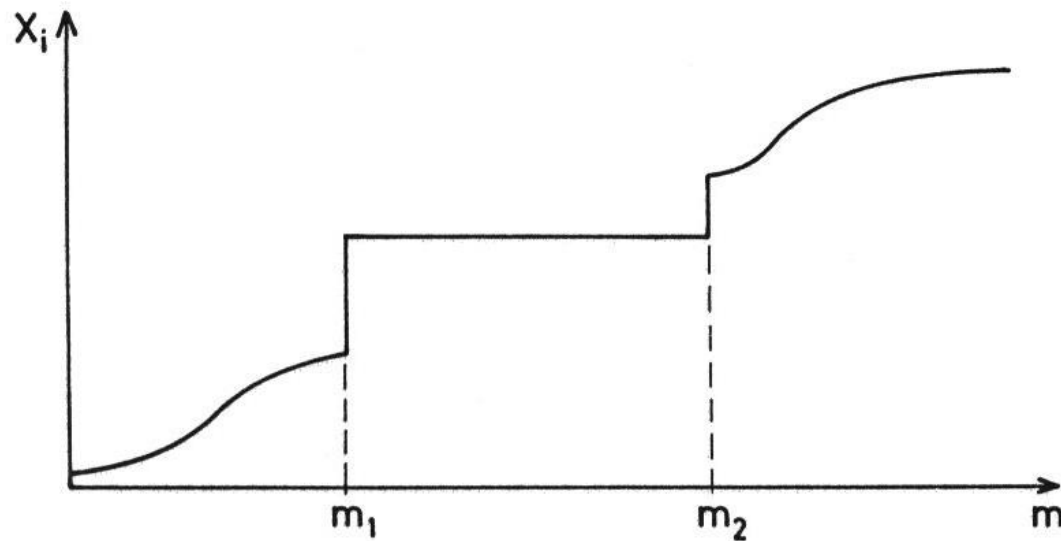
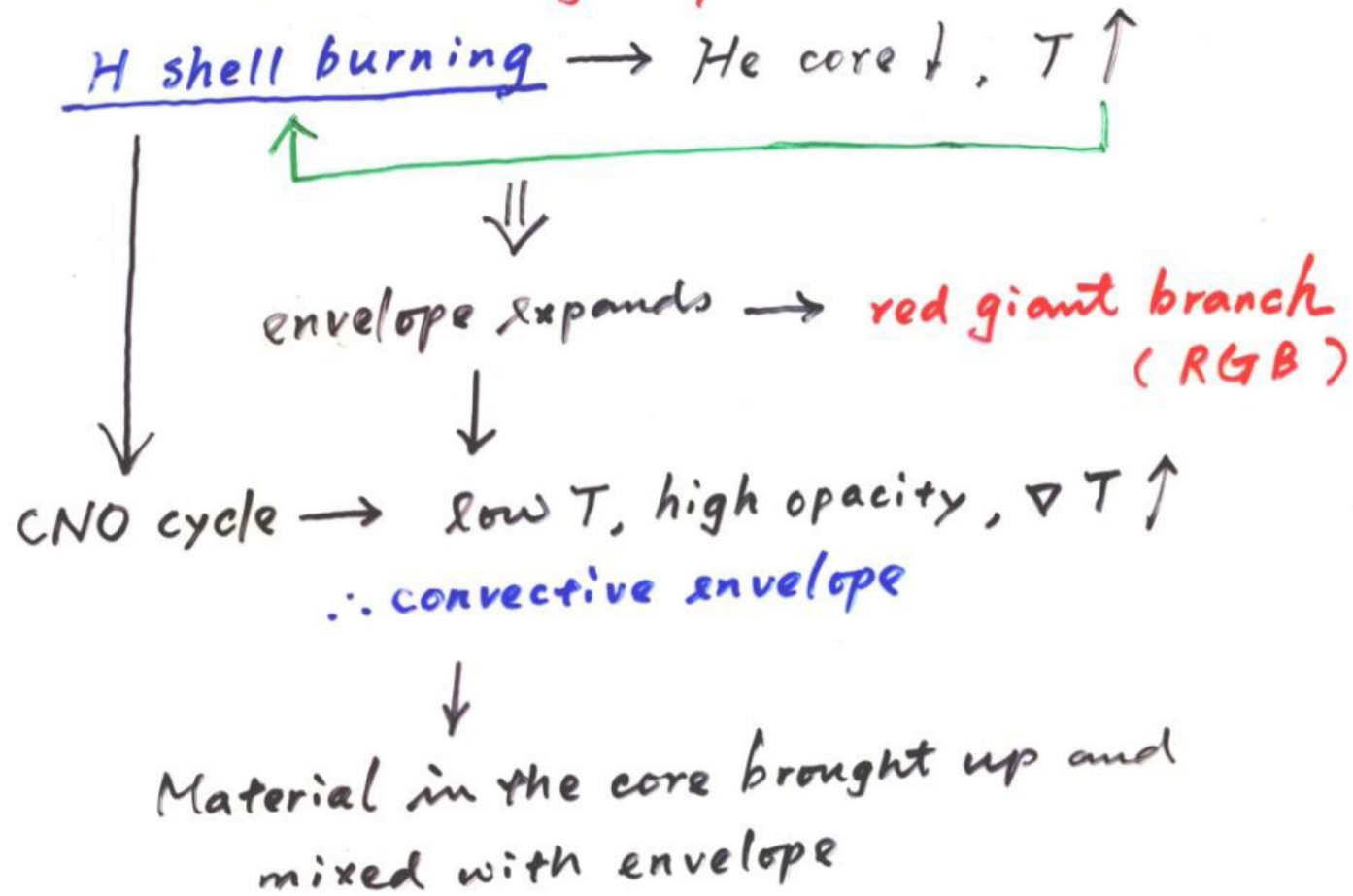


Fig.8.1. The abundances X_i are smeared out owing to rapid mixing inside a convection zone extending from m_1 to m_2 . At these borders X_i can be discontinuous

The Dredge-ups



⇒ The (first) dredge-up

photosphere observed N ↑ at the expenses of C and O

If $M > 0.5 M_{\odot} \rightarrow$ ^{He flash} He core burning (He "main sequence")
(lasting v. short)

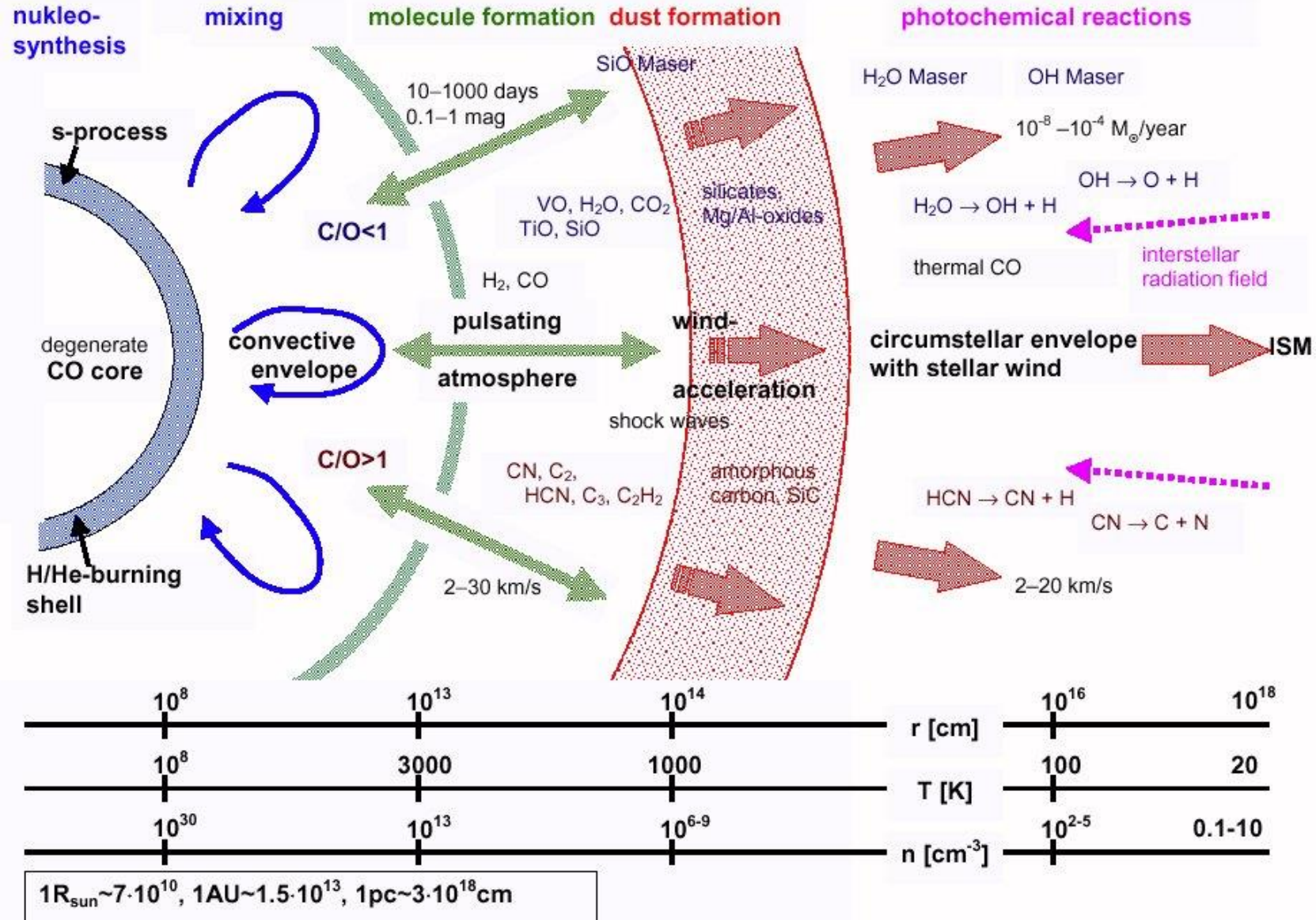
He shell burning \rightarrow asymptotic giant branch (AGB)

\Rightarrow The second dredge-up

\downarrow
 3α process \rightarrow unstable \rightarrow thermal pulses

Heavy elements in spectra of evolved stars
 \leftrightarrow YSOs \Rightarrow obs. test of stellar evolution

Schematic view of an AGB star

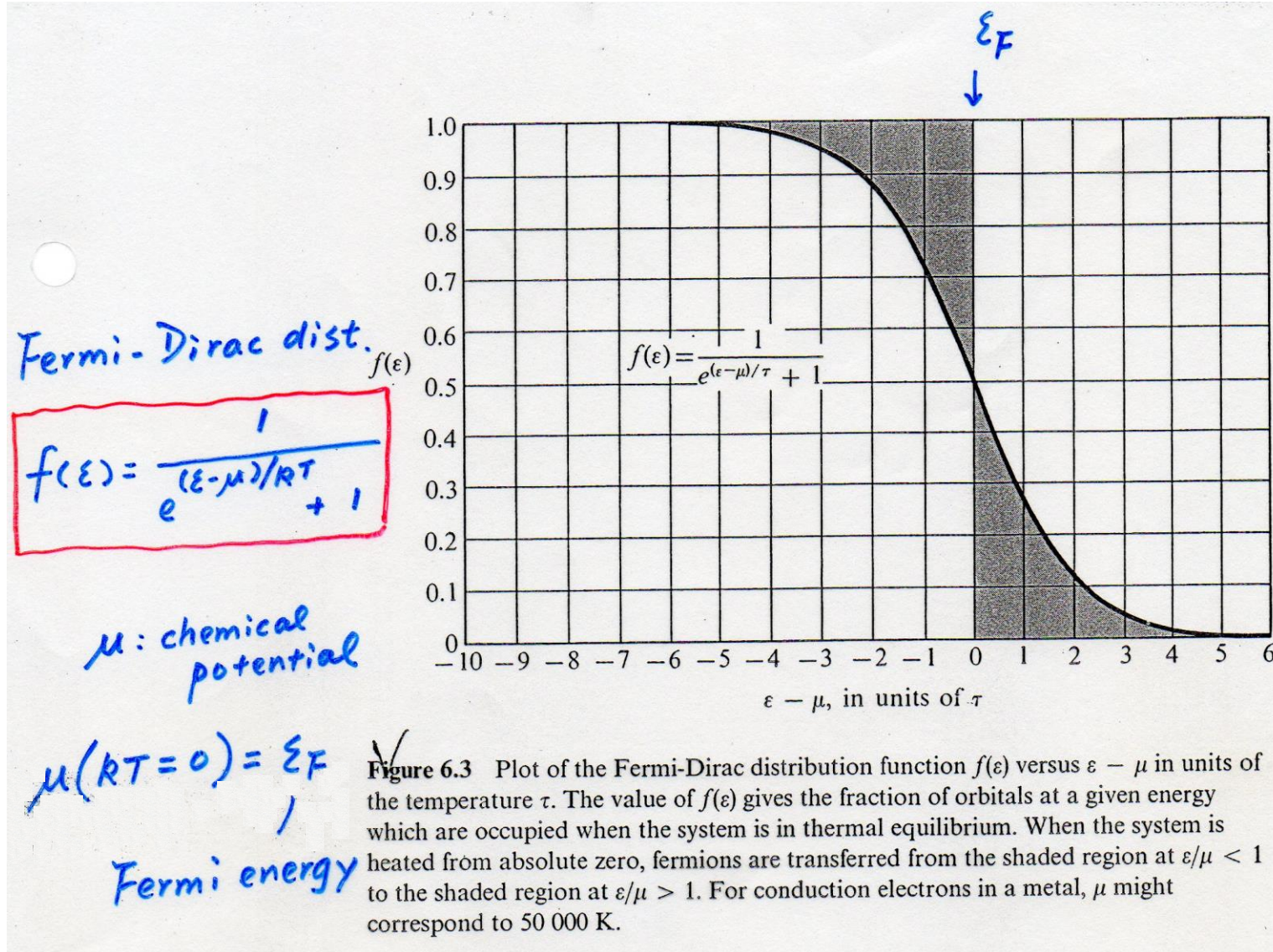


Electron Degeneracy

Fermi-Dirac distribution for non-interacting, indistinguishable particles obeying Pauli exclusion principle; applicable to half-integer spin in TE. Examples of fermions include the electron, proton, neutrons, ${}^3\text{He}$ ($2 e^{-}$, $2 p^{+}$, $1 n^0$)

Bose-Einstein distribution for particles not limited to single occupancy of the same energy state. i.e., that do not obey Pauli exclusion principle; with integer values of spin. Example bosons include ${}^4\text{He}$, the Higgs boson, gauge boson, graviton, meson.

A Fermi gas is called degenerate if the temperature is low in comparison with the Fermi temperature/energy.



Chemical Potential (μ)

- Temperature governs the flow of energy between two systems.
- Chemical potential governs the flow of particles; from higher chemical potential to the lower

Bose-Einstein dist.

$$f(\epsilon) = \frac{1}{e^{(\epsilon - \mu)/RT} - 1}$$

classical limit

$$f(\epsilon) \ll 1$$

$$f(\epsilon) = e^{-(\epsilon - \mu)/RT}$$

Maxwell-Boltzmann dist.

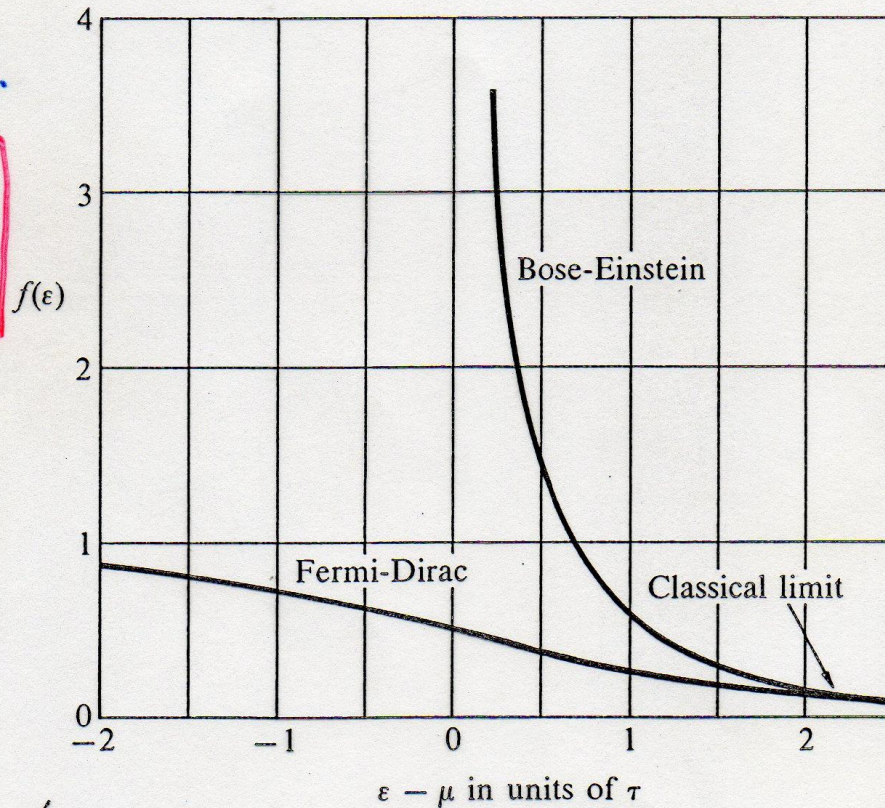


Figure 6.6 Comparison of Bose-Einstein and Fermi-Dirac distribution functions. The classical regime is attained for $(\epsilon - \mu) \gg \tau$, where the two distributions become nearly identical. We shall see in Chapter 7 that in the degenerate regime at low temperature the chemical potential μ for a FD distribution is positive, and changes to negative at high temperature.

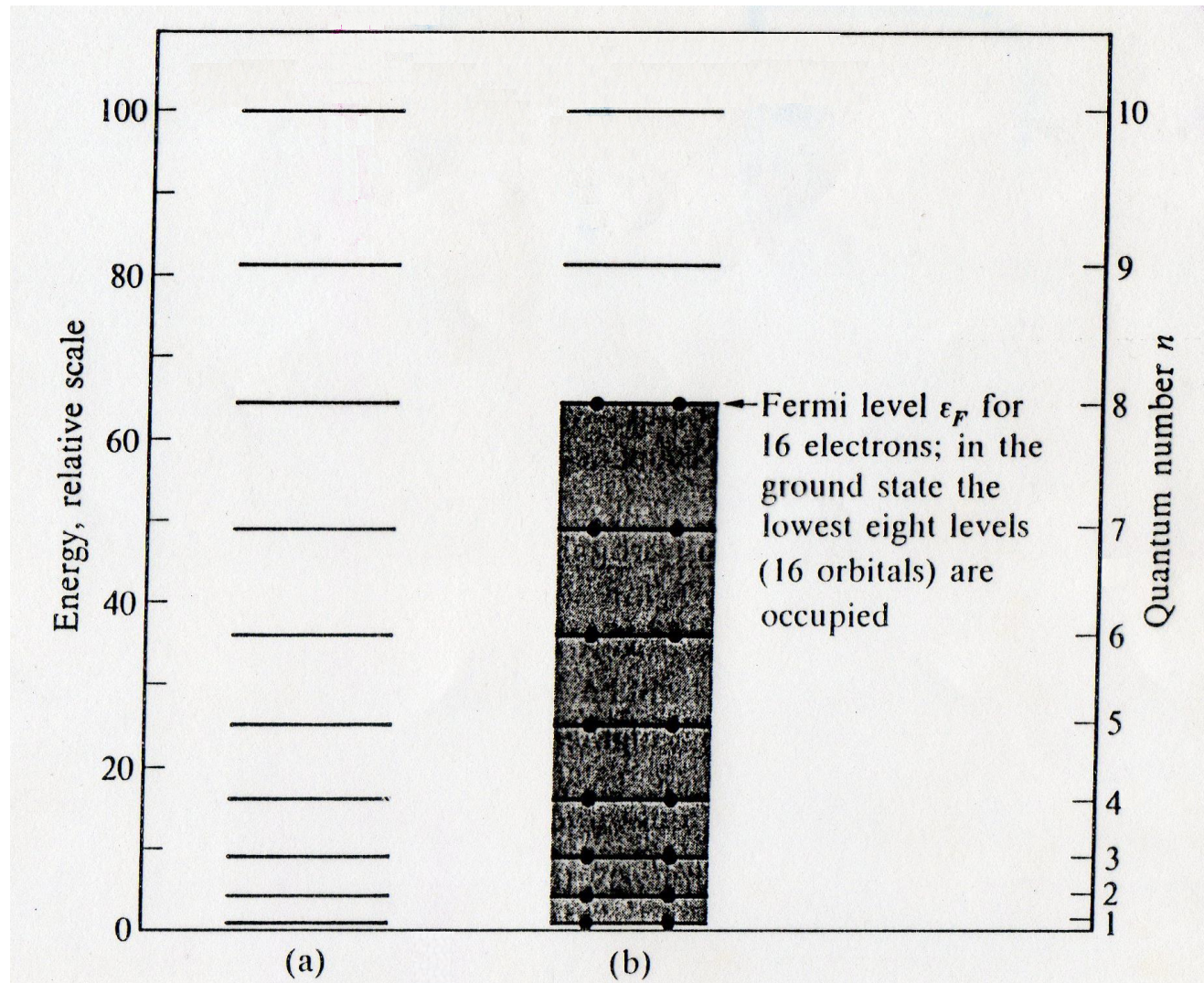


Figure 7.1 (a) The energies of the orbitals $n = 1, 2, \dots, 10$ for an electron confined to a line of length L . Each level corresponds to two orbitals, one for spin up and one for spin down. (b) The ground state of a system of 16 electrons. Orbitals above the shaded region are vacant in the ground state.

As time goes on, electron degeneracy^c becomes increasingly important,

e.g. $p_e^{\text{deg}} \sim 1.7\%$ of total pressure at $\tau \sim 0$
 $\sim 7.5\%$ " " $\tau \sim 9.2 \times 10^9 \text{ yr}$

Taking electron deg. pressure into account,

Misothermal core $\sim 0.13 M_{\odot}$

\Rightarrow pressure insufficient to support overlying layers

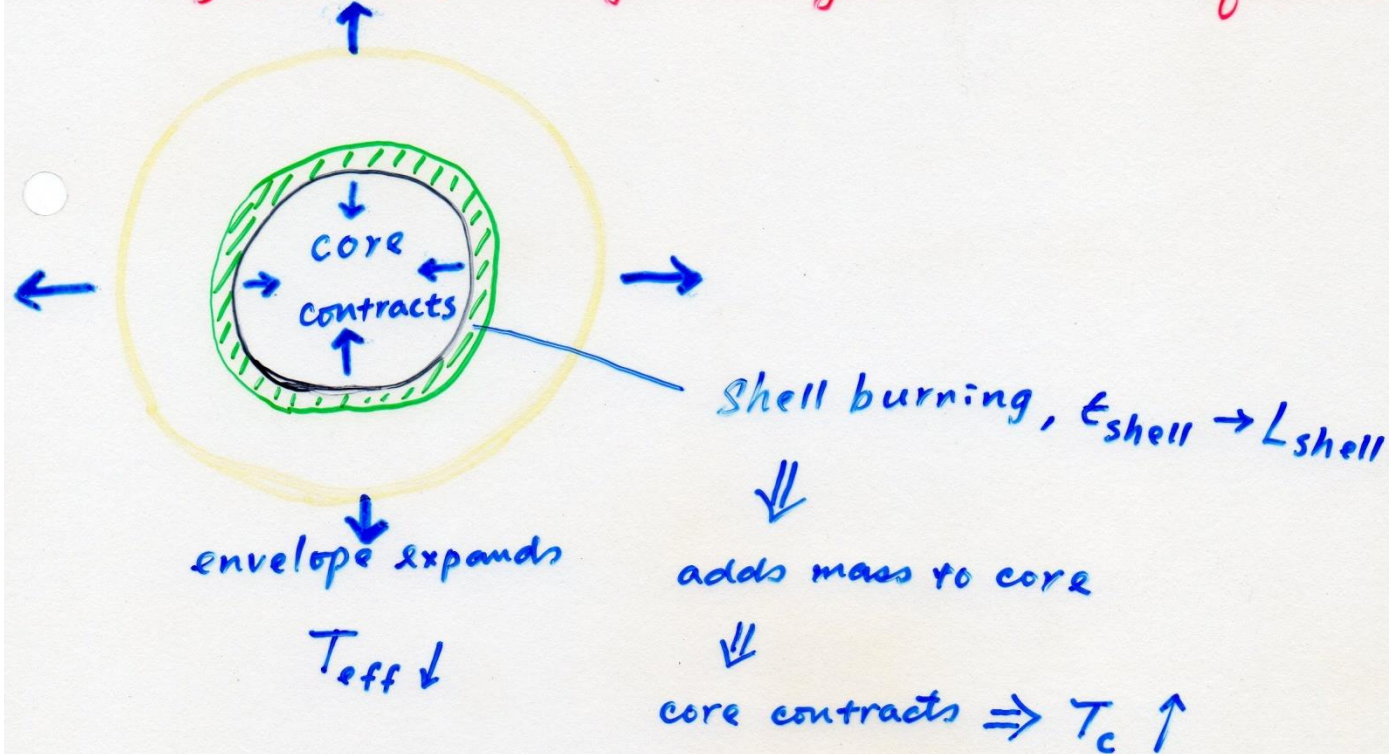
\Rightarrow core contraction \Rightarrow heated, $\epsilon_{\text{nuc}} \uparrow$

\Rightarrow Overlying layers pushed outwards

$\Rightarrow \epsilon_{\text{nuc}}$ in a narrowing shell

End of main-sequence phase

Structural changes during Post-Main Sequence



$$L_* \approx L_{\text{shell}}$$

L_{shell} heats core \rightarrow core \approx isothermal

\therefore needs density gradient to support against gravity

For low-mass stars ($0.7 - 2 M_{\odot}$)

ρ_c is high \rightarrow e^- degeneracy sets in before
core He burning begins

When He burning starts $\rightarrow T_c \uparrow$ (but ρ_c does not)

$\rightarrow \epsilon \uparrow \uparrow$

\Rightarrow He flash

$E_{\text{release}} \sim 10^{11} L_{\odot}$ in a few seconds

Energy absorbed by envelope (being pushed)


no observable effects!

WHY IS THERE A HELIUM FLASH?

normal ideal gas $P \uparrow \Rightarrow T \uparrow$

\therefore Energy input $\Rightarrow T \uparrow \Rightarrow P \uparrow \Rightarrow$ expand

stable
against thermal
instability



\Rightarrow a safety-valve mechanism

If the helium core is degenerate

$P \nleftrightarrow T$

when $T \gtrsim 10^8 \text{ K}$, $T \uparrow \Rightarrow$ runaway thermal
instability

within a few seconds, He ignited

\Rightarrow helium flash

The helium flash occurs for $M_{\text{core}} \approx 1 M_{\odot}$

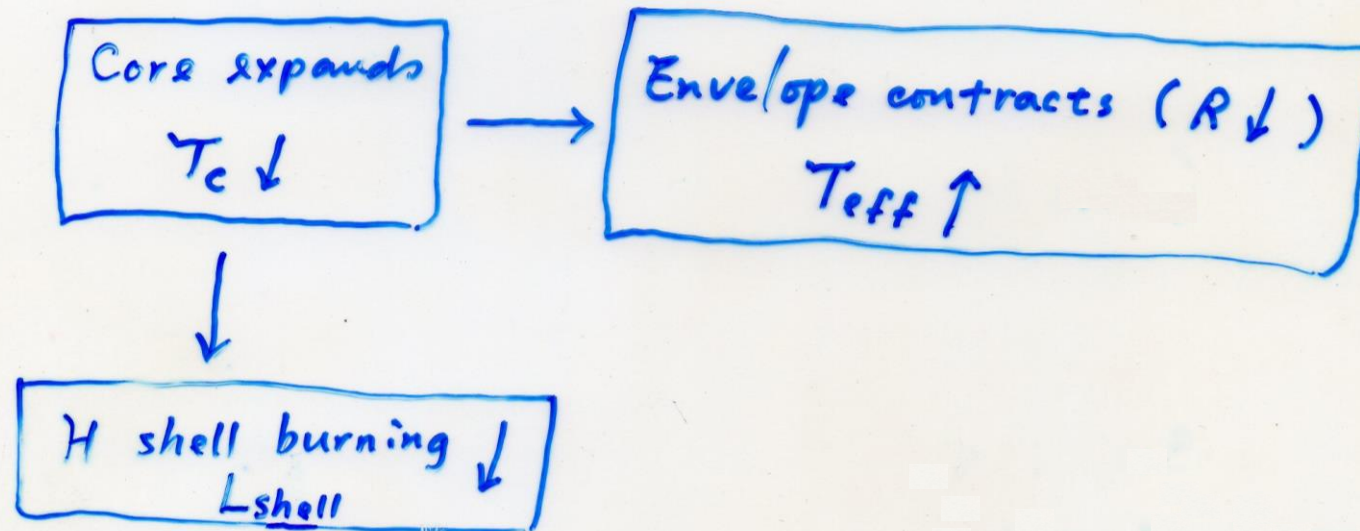
If $\mathcal{M} \leq 0.5 \mathcal{M}_{\odot}$ \rightarrow core never hot enough

If $\mathcal{M} \geq 2.25 \mathcal{M}_{\odot}$ \rightarrow core too hot, He ignited before a degenerate core develops

\rightarrow Only $\mathcal{M} \approx 0.5 - 2.25 \mathcal{M}_{\odot}$ stars experience the He flash.

After the helium flash

$T_c \uparrow \uparrow$, degeneracy lifted \rightarrow normal He burning



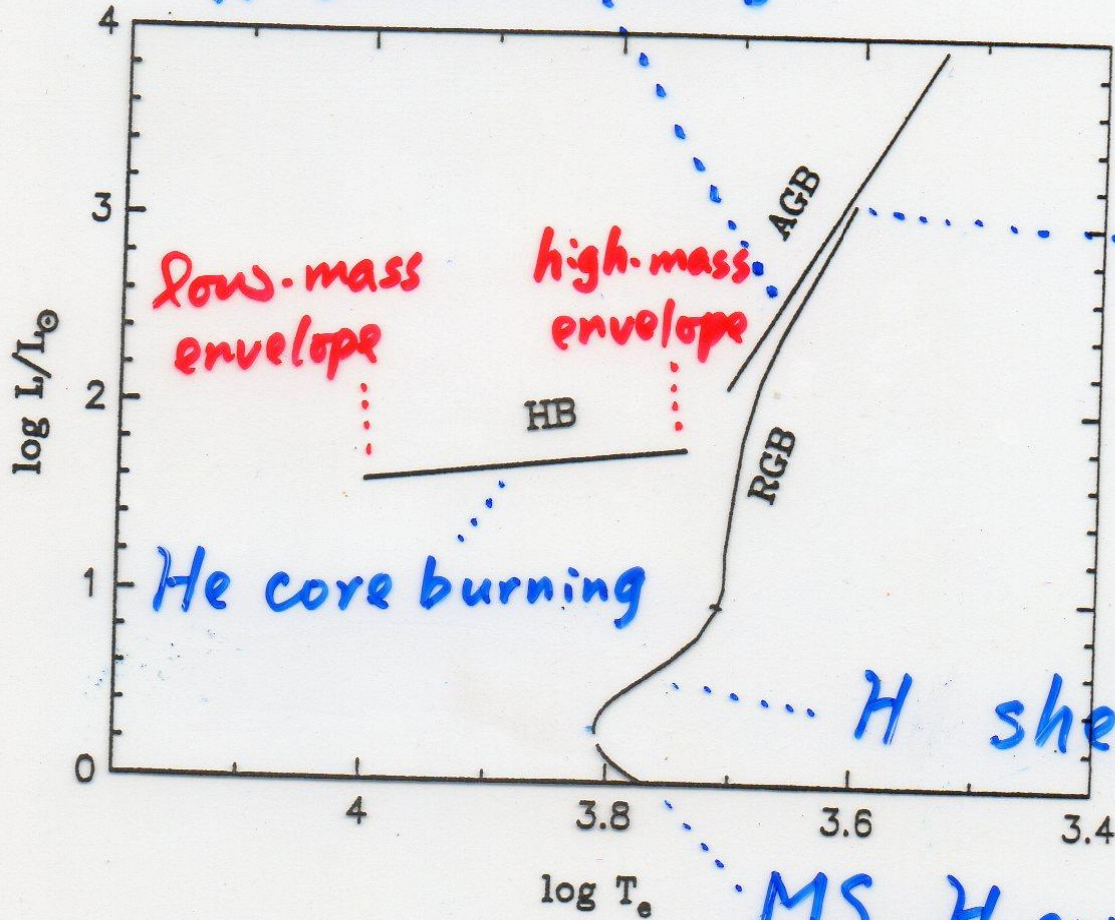
$\therefore R \downarrow, L_{shell}$

$\Rightarrow L_* \downarrow$, Star descends from RGB and moves to left in HRD

Core He burning is much shorter than the MS phase of core H burning, because He is short in abundance, not as efficient in energy supply (1/10 per mass), and the stellar luminosity is higher.

HB: $L \sim 50-100 L_{\odot}$, $\tau \sim 10^8$ yrs

core inert
He shell burning
H shell burning



M_{core} similar

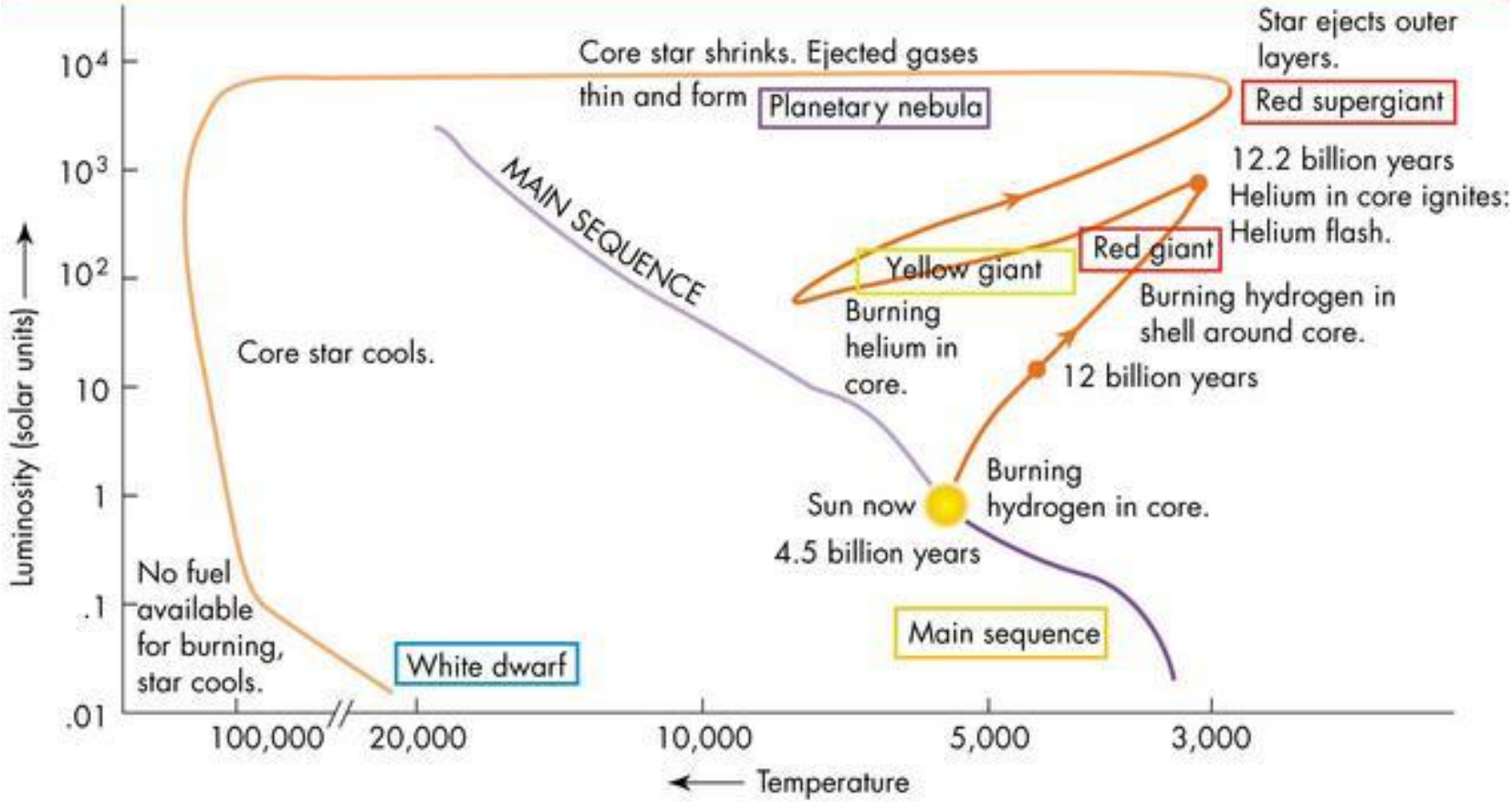
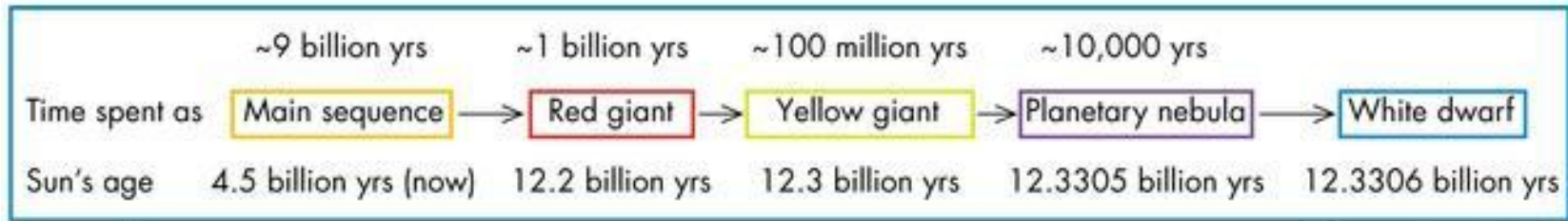
Tip of RGB
core He ignition

He core burning

core inert
H shell burning

MS H core burning

Figure 6.3. RGB, AGB, and HB in H-R diagram.



- ❑ MS (core H burning)
- ❑ Subgiant branch (shell H burning)
- ❑ Red giant branch (shell H burning)
- ❑ Red giant (core He flash)
- ❑ Horizontal branch (core He burning)
- ❑ Asymptotic giant branch (shell He burning)
- ❑ Red supergiant
- ❑ Protoplanetary nebula
- ❑ Planetary nebula
- ❑ White/black dwarf⁴⁷

Evolution of the Sun in the HRD

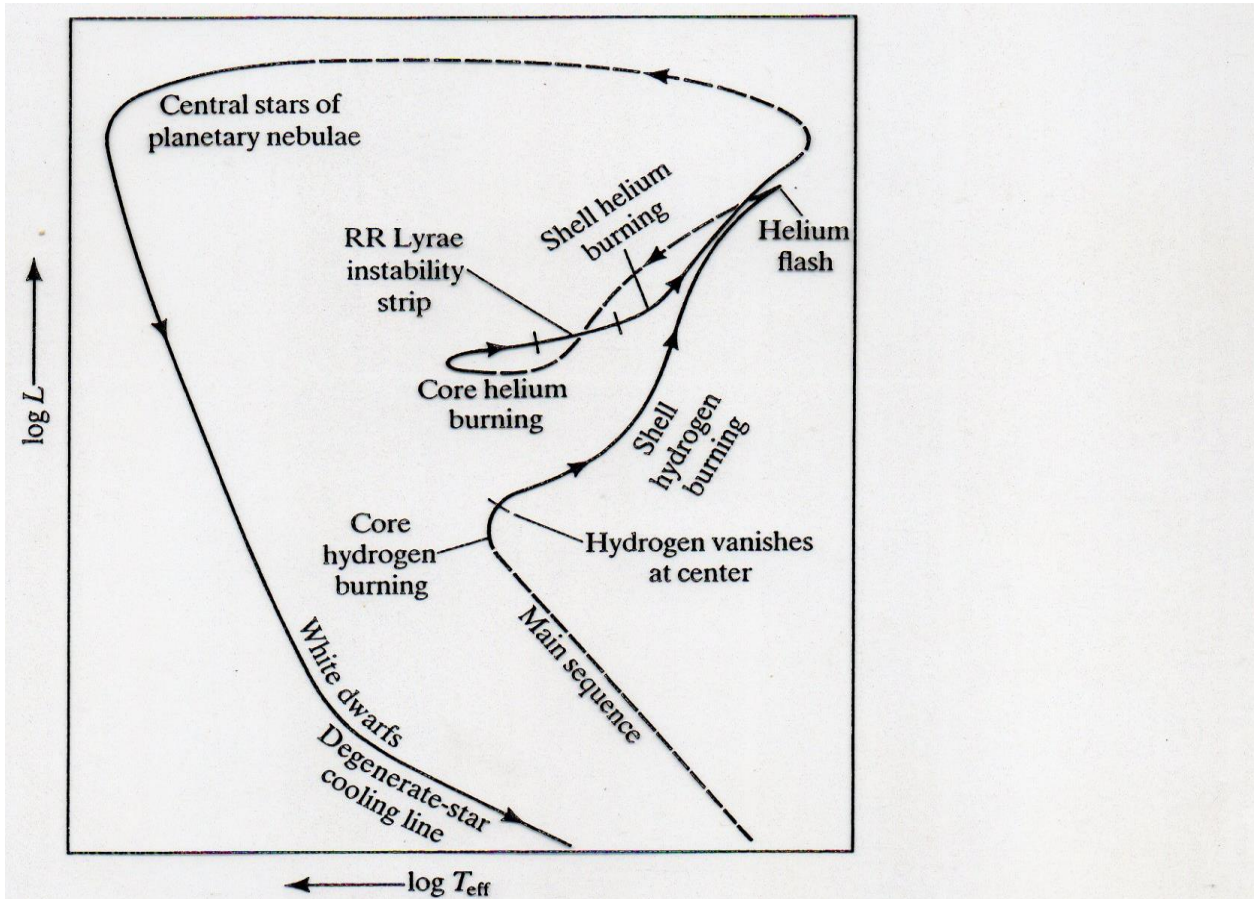
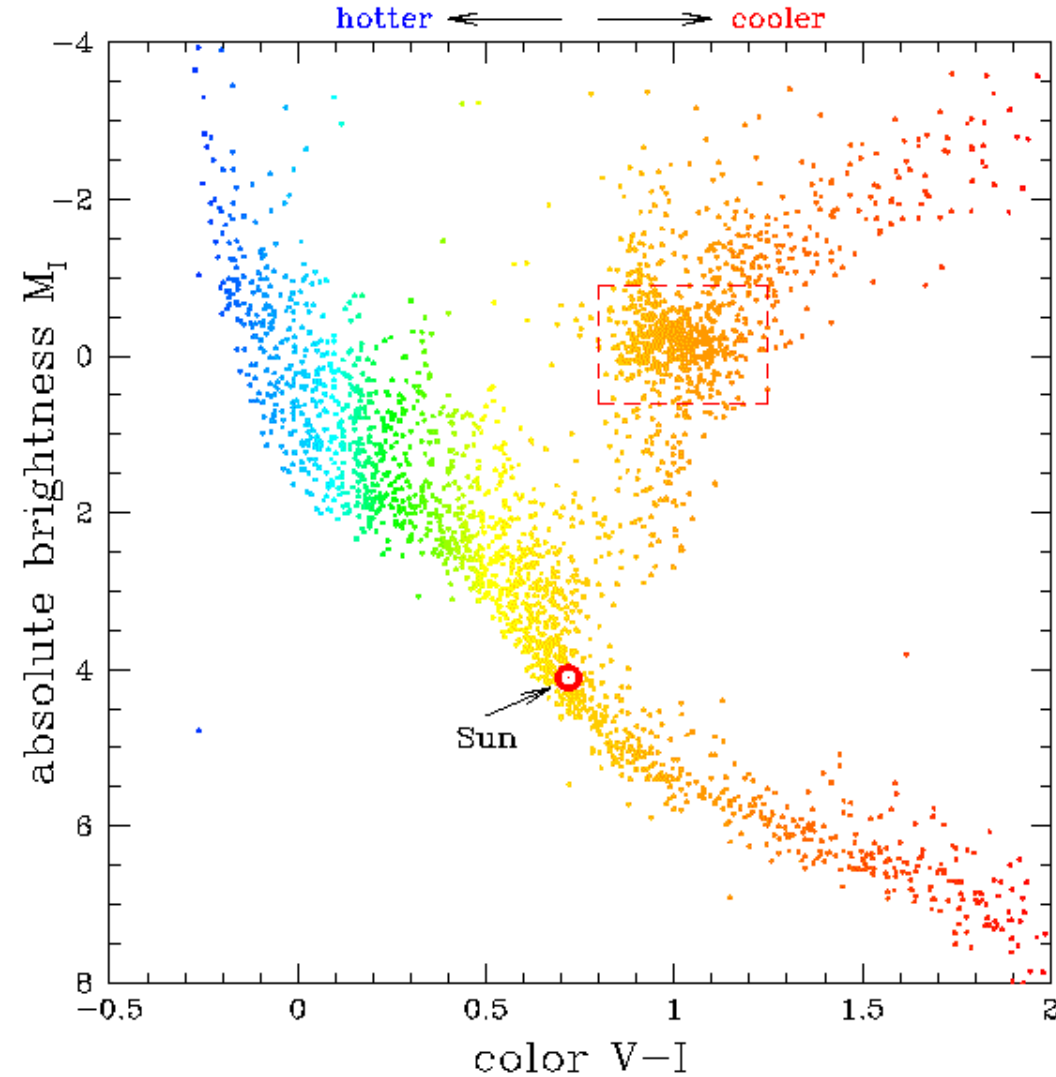


Figure 3-18. Schematic evolution track for a representative low-mass, globular-cluster star from the main sequence to its ultimate demise as a white dwarf. The major energy sources are indicated at several key phases. Dashed lines indicate episodes of very rapid evolution, during which details of the structure of the star are, at present, not too well known. Compare this figure with Figure 3-13.

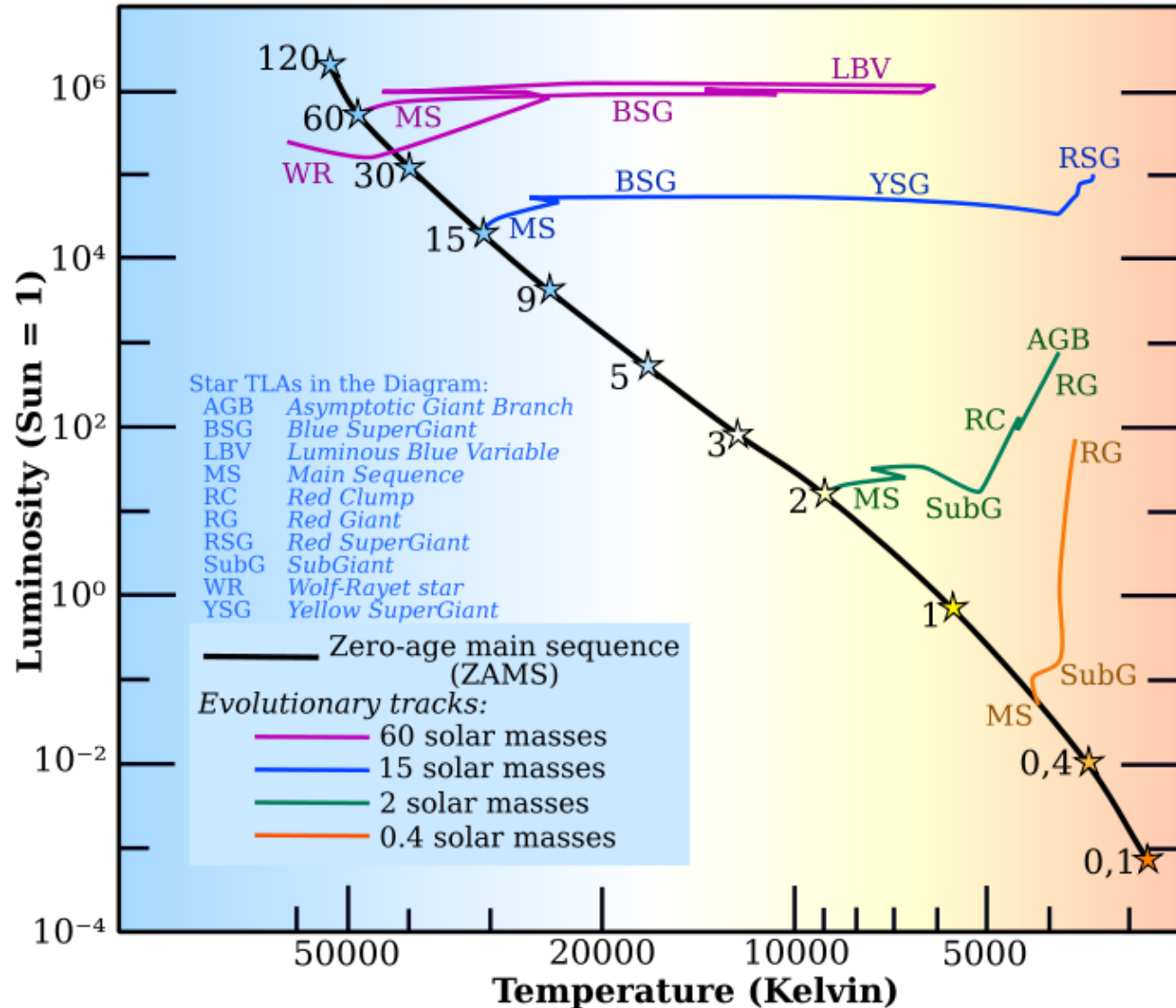
Mihalas & Binney

The **red** clump = HB (core He burning) of metal-rich stars



<http://www.astronomy.ohio-state.edu/~kstanek/CfA/RedClump/>

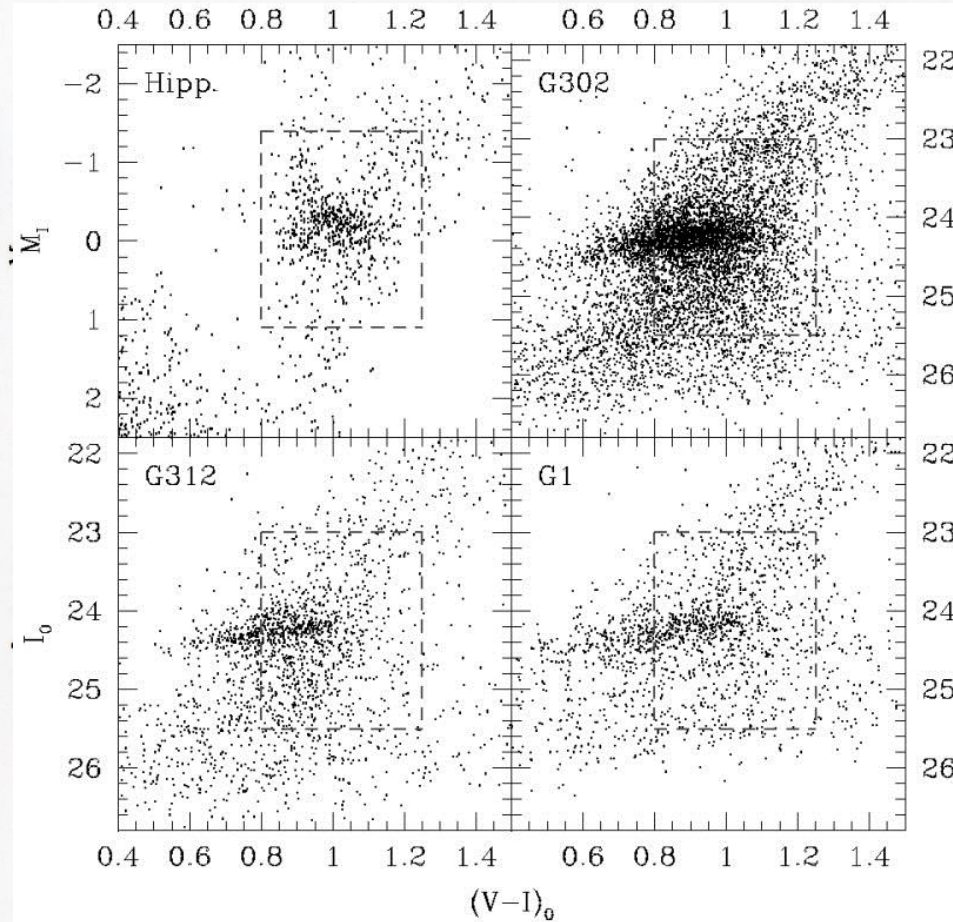
L_{RC} independent of composition or age \rightarrow standard candles



Distance to M31 With the *HST* and *Hipparcos* Red Clump Stars (1998)

K. Z. Stanek & P. M. Garnavich

$M_I = -0.23$



Using the red clump stars to determine the distance to M31

$$R_{M31} = \underbrace{784}_{\text{Statistical error}} \pm 13 \pm 17 \text{ kpc} \quad \begin{matrix} \text{Systematic} \\ \swarrow \\ \end{matrix}$$

Fig. 2.— The red clump dominated parts of CMDs for the *Hipparcos* stars (upper-left panel) and for three fields in M31 observed with the *HST*. The dashed rectangles surround the red clump regions used for the comparison between the local and the M31 red clump stars.

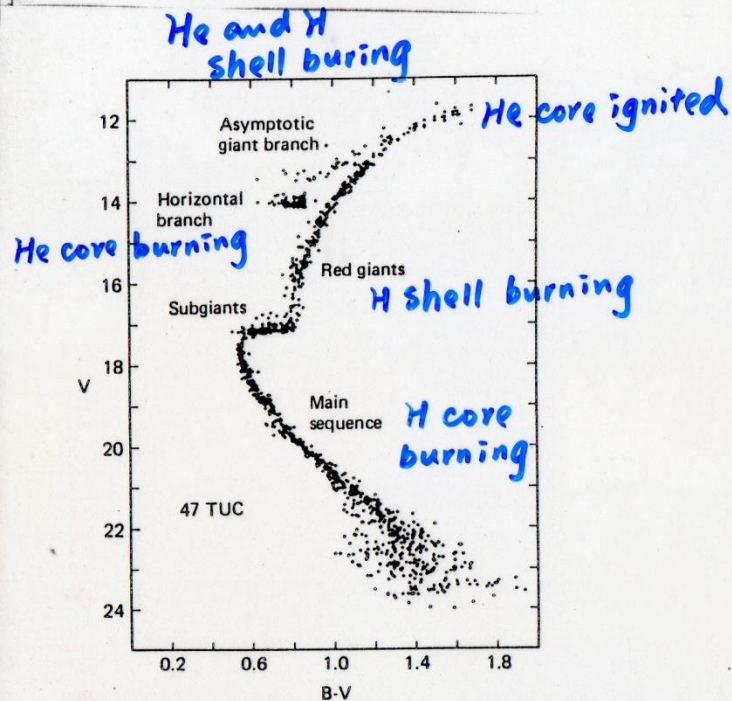


Fig. 1.7. The color apparent magnitude diagram for 47 Tucanae. The new measurements go down to stars as faint as 23rd magnitude, though for the faint stars the scatter becomes large. The main sequence and the giant and subgiant branches are surprisingly sharp, showing that there are very few or no binaries in this globular cluster. The red stub of the horizontal branch is seen at $V \sim 14$ and $B - V \sim 0.8$. The asymptotic giant branch (see Chapter 14) is seen above the horizontal branch. From Hesser *et al.* (1987).

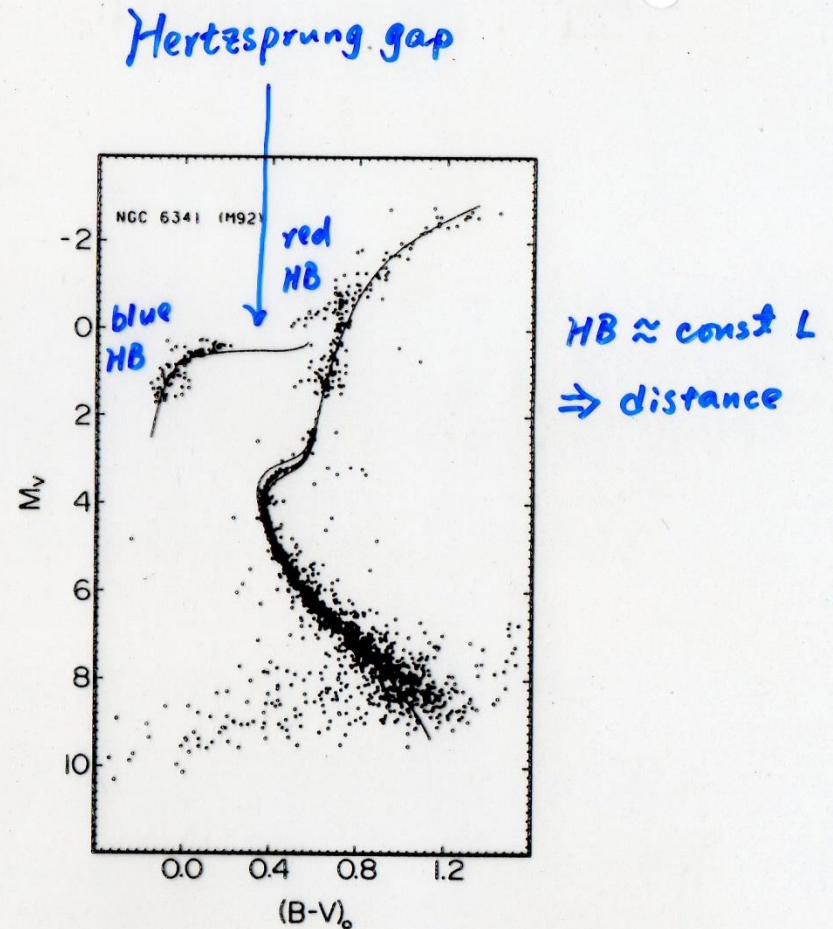


Fig. 1.8. The color absolute magnitude diagram for the globular cluster M92 (cluster 92 in the Messier catalog of nebulous objects). The new observations for M92, like those for 47 Tuc, go to very faint magnitudes. For M92 the main sequence is now clearly recognizable. In addition the subgiant, red giant and horizontal branches are clearly seen. Also seen is the so-called asymptotic branch, for $(B - V)_0 \sim 0.6$ above the horizontal branch. The thin lines shown are the theoretical isochrones, i.e. the location where stars are expected to be seen at a given time. From Hesser *et al.* (1987).

HB morphology differs from one GC to another.

MS Stars

$$M = \underline{1 - 9 M_{\odot}}$$

AGB

wind \rightarrow envelope

WD

\rightarrow C-O core $0.6 - 1.1 M_{\odot}$

roughly core mass \leftrightarrow MS mass

\Rightarrow expect WD mostly $0.6 M_{\odot}$

During AGB, H-shell and He-shell burning

bottom of He layer

Envelope shed = a random process in pulses

If H-shell burning → WD w/ a thin layer of H
80% of all DA white dwarfs

If He-shell burning (H lines, no He lines nor metal lines)

↓
less freq.

— WD He layer

DB (He I lines, no H, metals)
16%

⇒ expect more DA white dwarfs than DBs

obs 25% He lines

DC (continuous, no lines)

DO (He II lines)

DQ (C dominated)

- Origins of DA and non-DA uncertain: (1) exact phase when the last thermal pulse takes place after the AGB phase, or (2) convective mixing, radiative levitation, or diffusion.

$M = 0.7 - 1.0 M_{\odot}$
 $MS \rightarrow RG - He \text{ core} \lesssim 0.4 M_{\odot} \text{ WD}$
no AGB, PN phases

Mass distribution of DA white dwarfs in the First Data Release of the Sloan Digital Sky Survey

A&A 419, L5–L8 (2004)

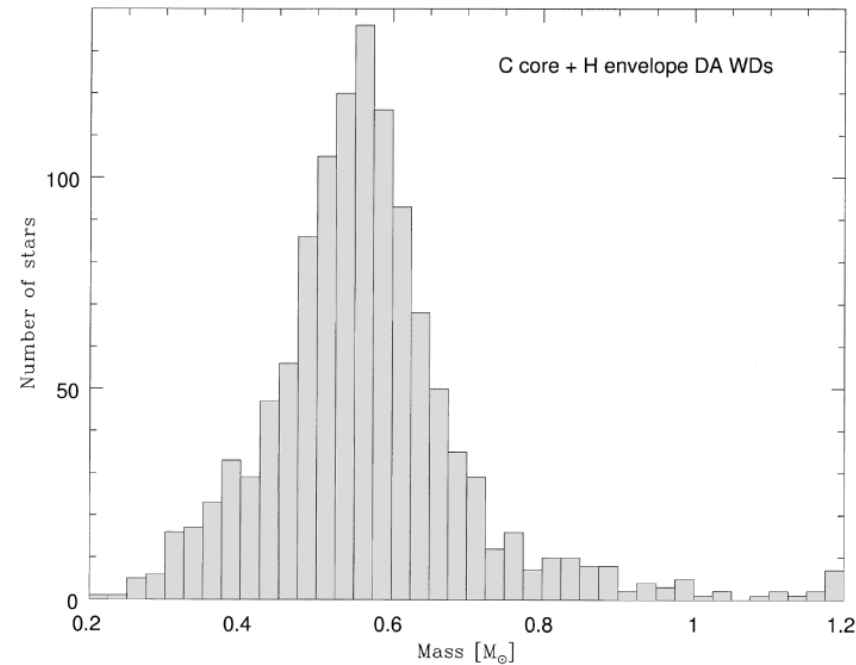
J. Madej¹, M. Należyty¹, and L. G. Althaus²

¹ Astronomical Observatory, University of Warsaw, Al. Ujazdowskie 4, 00-478 Warsaw, Poland

² Departament de Física Aplicada, Universitat Politècnica de Catalunya, Av. del Canal Olímpic s/n, 08860, Castelldefels, Spain

Received 4 March 2004 / Accepted 23 March 2004

Abstract. We investigate the sample of 1175 new nonmagnetic DA white dwarfs with the effective temperatures $T_{\text{eff}} \geq 12\,000$ K, which were extracted from the Data Release 1 of the Sloan Digital Sky Survey. We determined masses, radii, and bolometric luminosities of stars in the sample. The above parameters were derived from the effective temperatures T_{eff} and surface gravities $\log g$ published in the DR1, and the new theoretical $M - R$ relations for carbon-core and oxygen-core white dwarfs. Mass distribution of white dwarfs in this sample exhibits the peak at $M = 0.562 M_{\odot}$ (carbon-core stars), and the tail towards higher masses. Both the shape of the mass distribution function and the empirical mass-radius relation are practically identical for white dwarfs with either pure carbon or pure oxygen cores.



$\mathcal{M} < 0.7 M_{\odot}$

$< 0.16 M_{\odot} \rightarrow$ no RGB

$< 0.5 M_{\odot} \rightarrow \tau_{\text{MS}} > \tau_{\text{Universe}}$

$< 0.5 \sim 0.7 M_{\odot} \rightarrow$ no core He burning

Very low-mass stars are completely convective
 \rightarrow more H to burn $\rightarrow \tau_{\text{MS}}$ lengthened

A $1 M_{\odot}$ main sequence star

- $\tau_{\text{MS}} \sim 10^{10}$ yrs
- $\tau_{\text{RGB}} \sim 10^9$ yrs
- $\tau_{\text{HB}} \sim 10^8$ yrs
- $\tau_{\text{AGB}} \sim 2 \times 10^7$ yrs
- $\tau_{\text{PS}} \sim 5 \times 10^4$ yrs

A remnant of a 0.6 WD

$$\underline{\mathcal{M} < 25 M_{\odot}}$$

Mass loss rate low

$$\mathcal{M} = 20 - 25 M_{\odot}$$

O type star \rightarrow red supergiant \rightarrow supernova

$$\mathcal{M} < 20$$

O type star \rightarrow red supergiant \rightarrow Cepheid
 \rightarrow red supergiant \rightarrow supernova

$$\underline{\mathcal{M} = 25 - 60 M_{\odot}}$$

Mass loss not sufficient to remove the entire envelope

$$\mathcal{M} = 40 - 60 M_{\odot}$$

O type star \rightarrow blue super giant \rightarrow yellow supergiant
 \rightarrow red supergiant
 \rightarrow blue supergiant \rightarrow WN \rightarrow supernova

$$\mathcal{M} = 25 - 40 M_{\odot}$$

O type star \rightarrow blue super giant \rightarrow yellow supergiant
 \rightarrow red supergiant
 \rightarrow supernova

$\mathcal{M} > 60 M_{\odot}$

Mass loss fierce $\approx 10^{-1} M_{\odot} \text{ yr}^{-1}$, rid of almost entire envelope during the LBV stage, left with a WR star, evolving toward a SN.

O type star \rightarrow Of star \rightarrow blue super giant

\rightarrow luminous blue variable \rightarrow WN star

\rightarrow WC star \rightarrow supernova

I. A non-rotating $60 M_{\odot}$ star from the zero-age main sequence to the pre-supernova stage^{★,★★}

Jose H. Groh¹, Georges Meynet¹, Sylvia Ekström¹, and Cyril Georgy²

¹ Geneva Observatory, Geneva University, Chemin des Maillettes 51, 1290 Sauverny, Switzerland
e-mail: jose.groh@unige.ch

² Astrophysics group, EPSAM, Keele University, Lennard-Jones Labs, Keele, ST5 5BG, UK

ABSTRACT

For the first time, the interior and spectroscopic evolution of a massive star is analyzed from the zero-age main sequence (ZAMS) to the pre-supernova (SN) stage. For this purpose, we combined stellar evolution models using the Geneva code and stellar atmospheric/wind models using CMFGEN. With our approach, we were able to produce observables, such as a synthetic high-resolution spectrum and photometry, thereby aiding the comparison between evolution models and observed data. Here we analyze the evolution of a non-rotating $60 M_{\odot}$ star and its spectrum throughout its lifetime. Interestingly, the star has a supergiant appearance (luminosity class I) even at the ZAMS. We find the following evolutionary sequence of spectral types: O3 I (at the ZAMS), O4 I (middle of the H-core burning phase), B supergiant (BSG), B hypergiant (BHG), hot luminous blue variable (LBV; end of H-core burning), cool LBV (H-shell burning through the beginning of the He-core burning phase), rapid evolution through late WN and early WN, early WC (middle of He-core burning), and WO (end of He-core burning until core collapse). We find the following spectroscopic phase lifetimes: 3.22×10^6 yr for the O-type, 0.34×10^5 yr (BSG), 0.79×10^5 yr (BHG), 2.35×10^5 yr (LBV), 1.05×10^5 yr (WN), 2.57×10^5 yr (WC), and 3.80×10^4 yr (WO). Compared to previous studies, we find a much longer (shorter) duration for the early WN (late WN) phase, as well as a long-lived LBV phase. We show that LBVs arise naturally in single-star evolution models at the end of the MS when the mass-loss rate increases as a consequence of crossing the bistability limit. We discuss the evolution of the spectra, magnitudes, colors, and ionizing flux across the star's lifetime, and the way they are related to the evolution of the interior. We find that the absolute magnitude of the star typically changes by ~ 6 mag in optical filters across the evolution, with the star becoming significantly fainter in optical filters at the end of the evolution, when it becomes a WO just a few 10^4 years before the SN explosion. We also discuss the origin of the different spectroscopic phases (i.e., O-type, LBV, WR) and how they are related to evolutionary phases (H-core burning, H-shell burning, He-core burning).

Read the first 4 paragraphs of this paper.⁷¹

Stellar Rotation

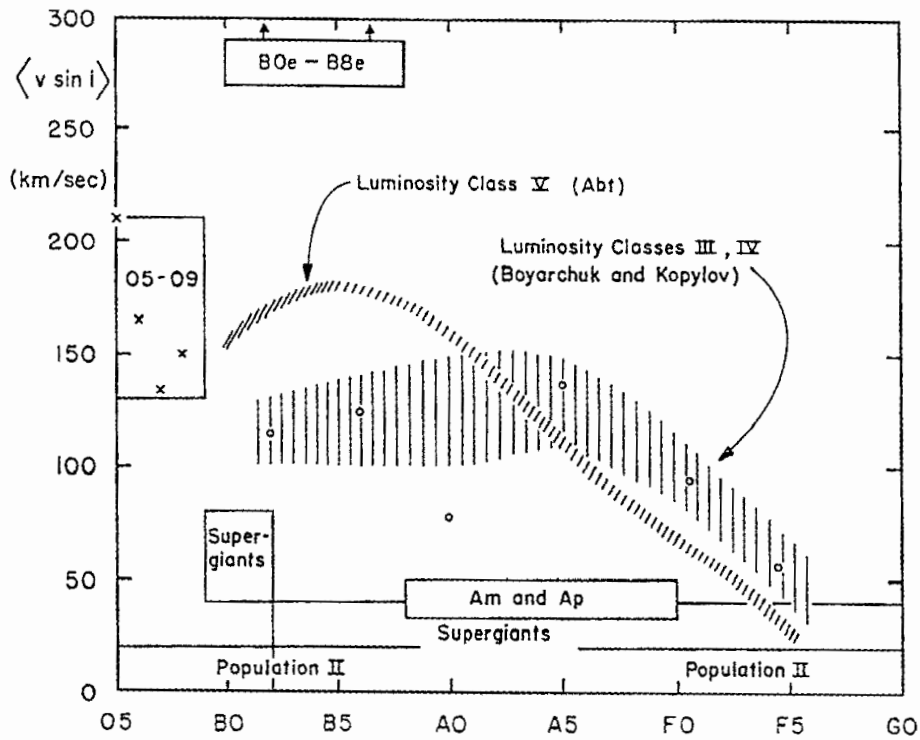
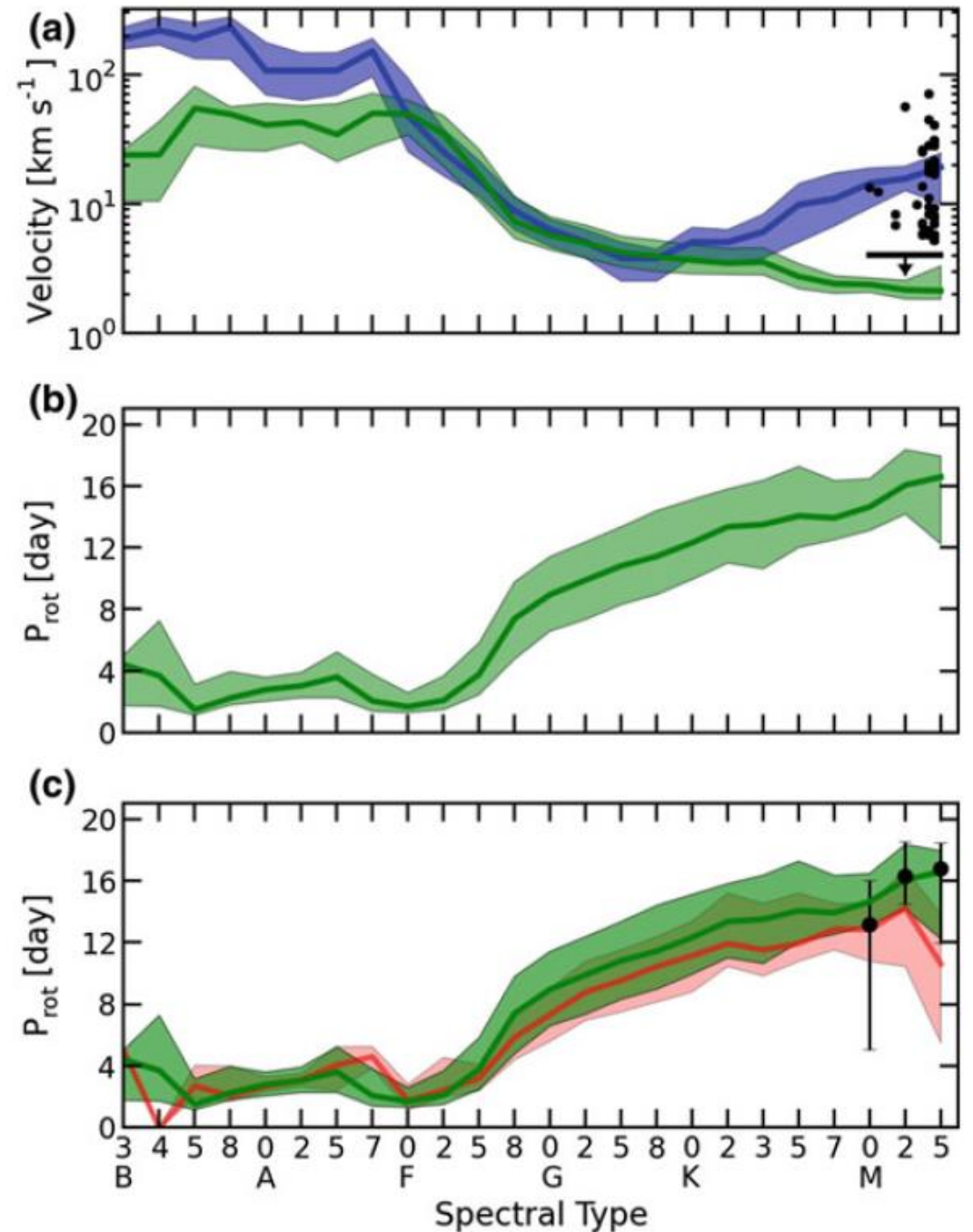


Fig. 3. Projected equatorial velocities, averaged over all possible inclinations, as a function of spectral type. On the main sequence (luminosity class V), early-type stars have rotational velocities that reach and even exceed 200 km/s; these velocities drop to a few km/s for late-type stars, such as the Sun (type G2) (Slettebak [20]; courtesy Gordon & Breach)

Fig. 2.2 *Panel A* The blue curve is the median equatorial velocity $(4/\pi) \langle v \sin i \rangle$ for each spectral type from Glebocki and Gnacinski (2005). The green curve shows the equatorial velocity of the *Kepler* targets, $\bar{v}(s.t.)$, derived from the measured rotation periods and the KIC radii. The black points show measurements by Reiners and Mohanty (2012). In this sample 201 stars have an upper $v \sin i$ limit of 4 km/s (due to instrumental limitations), these stars are represented by the solid bar. *Panel B* The rotation periods P_{rot} of the stars in our sample, averaged within each spectral type. *Panel C* The same as panel B, but for comparison we show the median of the rotation periods measured by McQuillan et al. (2013) (black points with errorbars), for the stars overlapping with our sample. Similarly, the red curve shows the median of the rotation periods found by Debosscher et al. (2011). Shaded areas and error bars span the upper and lower 34th percentile values from the median. Reproduced with permission from Astronomy & Astrophysics, © ESO



Rotation → star cooler and fainter

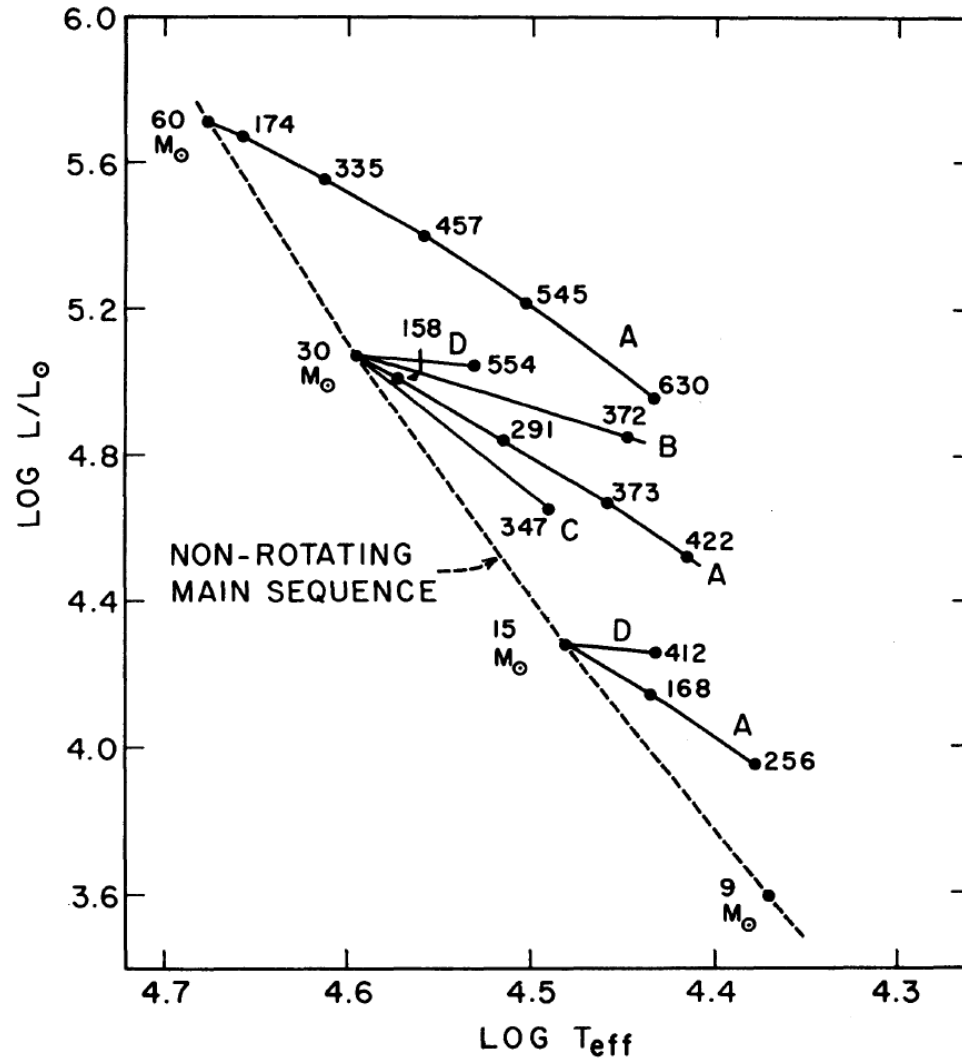


FIG. 2.—Theoretical H-R diagram showing model sequences of increasing angular momentum (*solid curves*). Numbers on curves give calculated velocities at the equator in km sec^{-1} . The distribution of angular momentum for each sequence is indicated by the letter A, B, C, or D.

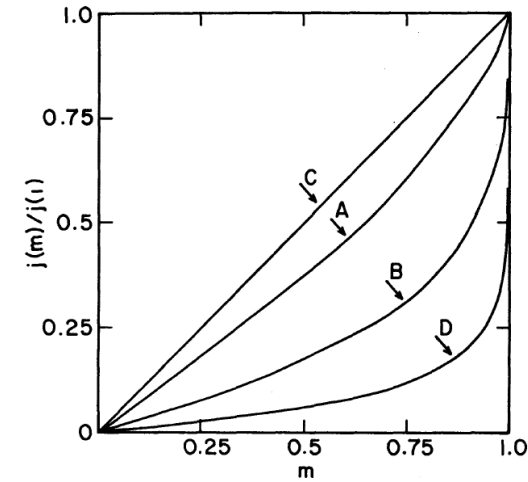


FIG. 1.—Angular momentum per unit mass, as a function of mass fraction interior to a given cylinder about the axis of rotation, for three assumed laws of differential rotation (Cases A, B, and C) and for a uniformly rotating model (Case D) of $30 M_{\odot}$, $\log J = 52.73$.

D: solid body rotation

Rotation law:

angular momentum distribution $j(m_w)$ as a function of, m_w , the mass fraction interior to the cylinder of radius w about the rotation axis.

1. Introduction

Massive stars are essential constituents of stellar populations and galaxies in the near and far Universe. They are among the most important sources of ionizing photons, energy, and some chemical species, which are ejected into the interstellar medium through powerful stellar winds and during their extraordinary deaths as supernovae (SN) and long gamma-ray bursts (GRB). For these reasons, massive stars are often depicted as cosmic engines, because they are directly or indirectly related to most of the major areas of astrophysical research.

Despite their importance, our current understanding of massive stars is still limited. This inconvenient shortcoming can be explained by many reasons on which we elaborate below. First, the physics of star formation mean that massive stars are rare ([Salpeter 1955](#)). Moreover, their lifetime is short, of a few to tens of millions of years (e.g., [Ekström et al. 2012](#); [Langer 2012](#)). These factors make it challenging to construct

evolutionary sequences and relate different classes of massive stars. This is in sharp contrast to what can be done for low-mass stars.

Second, one can also argue that the evolution of massive stars is extremely sensitive to the effects of some physical processes, such as mass loss and rotation ([Maeder & Meynet 2000](#); [Heger et al. 2000](#)), that have relatively less impact on the evolution of low-mass stars. However, the current implementation of rotation in one-dimensional codes relies on parametrized formulas, and the choice of the diffusion coefficients has a key impact on the evolution ([Meynet et al. 2013](#)). Likewise, mass-loss recipes arising from first principles are only available for main sequence (MS) objects ([Vink et al. 2000, 2001](#)) and a restricted range of Wolf-Rayet (WR) star parameters ([Gräfener & Hamann 2008](#)). Third, binarity seems to affect the evolution of massive stars, given that a large portion of them are in binary systems that will interact during the evolution ([Sana et al. 2012](#)).

Fourth, our understanding of different classes of stars is often built by comparing evolutionary models and observations. However, mass loss may affect the spectra, magnitudes, and colors of massive stars, thus making the comparison between evolutionary models and observations a challenge. In addition to luminosity, effective temperature, and surface gravity, the

observables of massive stars can be strongly influenced by a radiatively driven stellar wind that is characteristic of these stars. The effects of mass loss on the observables depend on the initial mass and metallicity, since they are in general more noticeable in MS stars with large initial masses, during the post-MS phase, and at high metallicities. When the wind density is significant, the mass-loss rate, wind clumping, wind terminal velocity, and velocity law have a strong impact on the spectral morphology. This makes the analysis of a fraction of massive stars a difficult task, and obtaining their fundamental parameters, such as luminosity and effective temperature, is subject to the uncertainties that comes from our limited understanding of mass loss and clumping. Furthermore, the definition of effective temperature of massive stars with dense winds is problematic and, while referring to an optical depth surface, it does not relate to a hydrostatic surface. This is caused by the atmosphere becoming extended, with the extension being larger the stronger the wind is. Stellar evolution models are able to predict the stellar parameters only up to the stellar hydrostatic surface, which is not directly reached by the observations of massive stars when a dense stellar wind is present. Since current evolutionary models do not thoroughly simulate the physical mechanisms happening at the atmosphere and wind, model predictions of the evolution of massive stars are difficult to be directly compared to observed quantities, such as a spectrum or a photometric measurement.

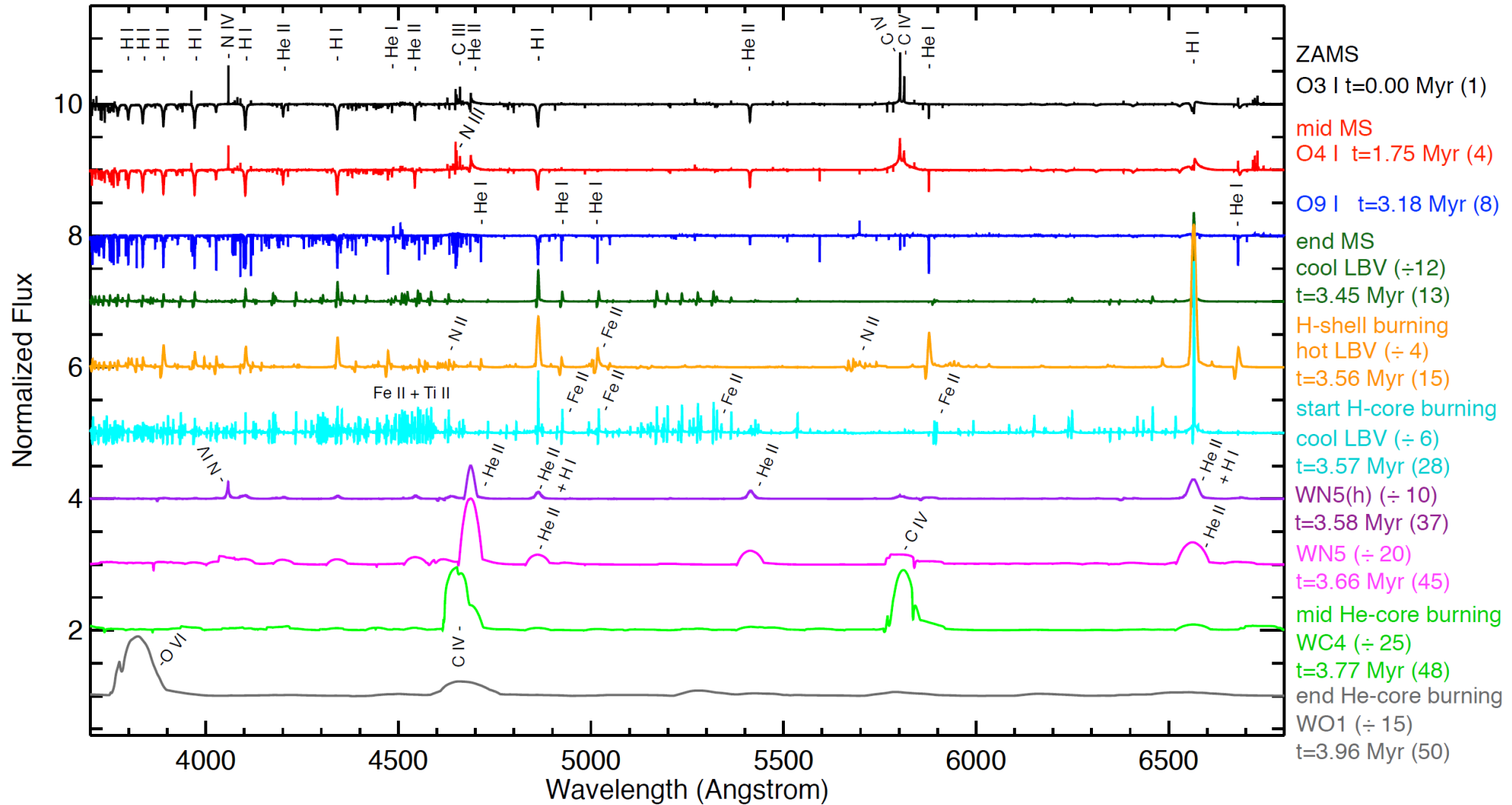


Fig. 4. Evolution of the ultraviolet **a)** (*top*) and optical spectra **b)** (*bottom*) of a non-rotating $60 M_{\odot}$ star. The evolution proceeds from top to bottom, with labels indicating the evolutionary phase, spectral type, scale factor when appropriate, age, and model stage according to Table 1. Note that certain spectra have been scaled for the sake of displaying the full range of UV and optical emission lines.

Initial Mass Function

The birthrate function $B(M, t)$ is the number of stars per unit volume, with masses between M and $M + dM$ that are formed out of ISM during time interval t and $t + dt$.

$$B(M, t) dM dt = \psi(t) \xi(M) dM dt,$$

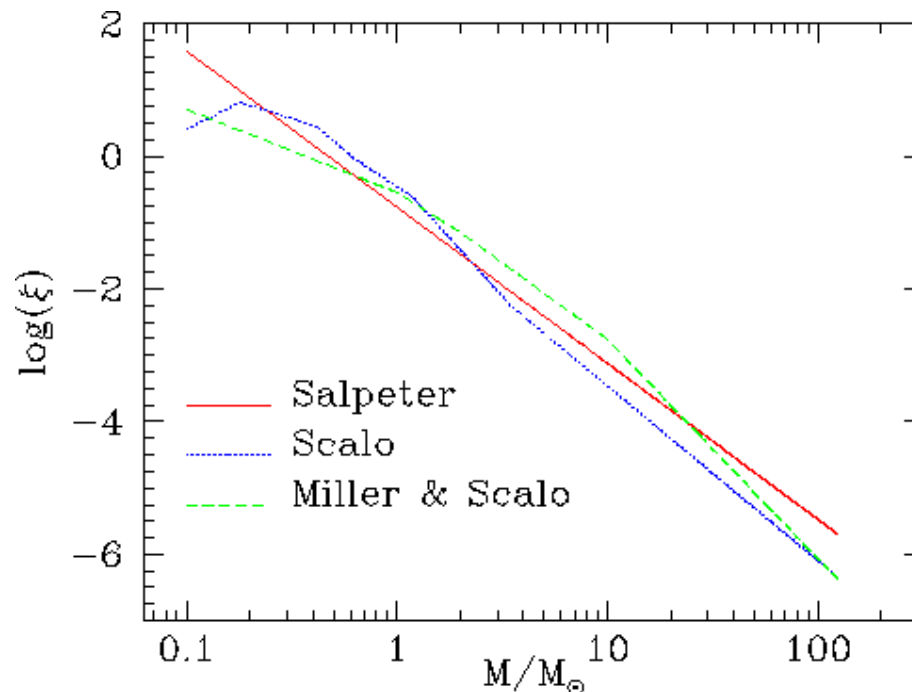
where $\psi(t)$ is the **star formation rate** (SFR), and $\xi(M)$ is the **initial mass function** (IMF).

For the Galactic disk, SFR is $5.0 \pm 0.5 M_{\odot} \text{pc}^{-2} \text{Gyr}^{-1}$ integrated over the z direction.

IMF: many more low-mass stars than higher mass stars as a result of cloud fragmentation?

The IMF specifies the fractional distribution in mass of a newly formed stellar system. It is often assumed to have a simple power law $\xi(M) = c M^{-\alpha} = c M^{-(1+\Gamma)}$

In general, $\xi(M)$ extends from a lower to an upper cutoff, e.g., from 0.1 to 125 solar masses. Commonly used IMFs are those of Salpeter (1955), Scalo (1986), and Miller and Scalo (1979).



- Edwin Salpeter (1955) on solar-neighborhood stars (ApJ, 121, 161)
Present-day LF \rightarrow mass-luminosity relation \rightarrow present-day mass function \rightarrow stellar evolution \rightarrow initial mass function
 $\alpha=2.35$ or $\Gamma = 1.35$
- Glenn E. Miller and John M. Scalo extended work below $1 M_{\odot}$
(1979, ApJS, 41, 513) $\alpha \approx 0$ for $M < 1 M_{\odot}$
- Pavel Kroupa (2002, Sci, 295, 82)
 $\alpha = 2.3$ for $M > 0.5 M_{\odot}$
 $\alpha = 1.3$ for $0.08 M_{\odot} < M < 0.5 M_{\odot}$
 $\alpha = 0.3$ for $M < 0.08 M_{\odot}$
- A universal IMF among stellar systems (SFRs, star clusters, galaxies) (Bastian et al. 2010, ARAA). But why?

THE LUMINOSITY FUNCTION AND STELLAR EVOLUTION

EDWIN E. SALPETER*

Australian National University, Canberra, and Cornell University

Received July 29, 1954

ABSTRACT

The evolutionary significance of the observed luminosity function for main-sequence stars in the solar neighborhood is discussed. The hypothesis is made that stars move off the main sequence after burning about 10 per cent of their hydrogen mass and that stars have been created at a uniform rate in the solar neighborhood for the last five billion years.

Using this hypothesis and the observed luminosity function, the rate of star creation as a function of stellar mass is calculated. The total number and mass of stars which have moved off the main sequence is found to be comparable with the total number of white dwarfs and with the total mass of all fainter main-sequence stars, respectively.

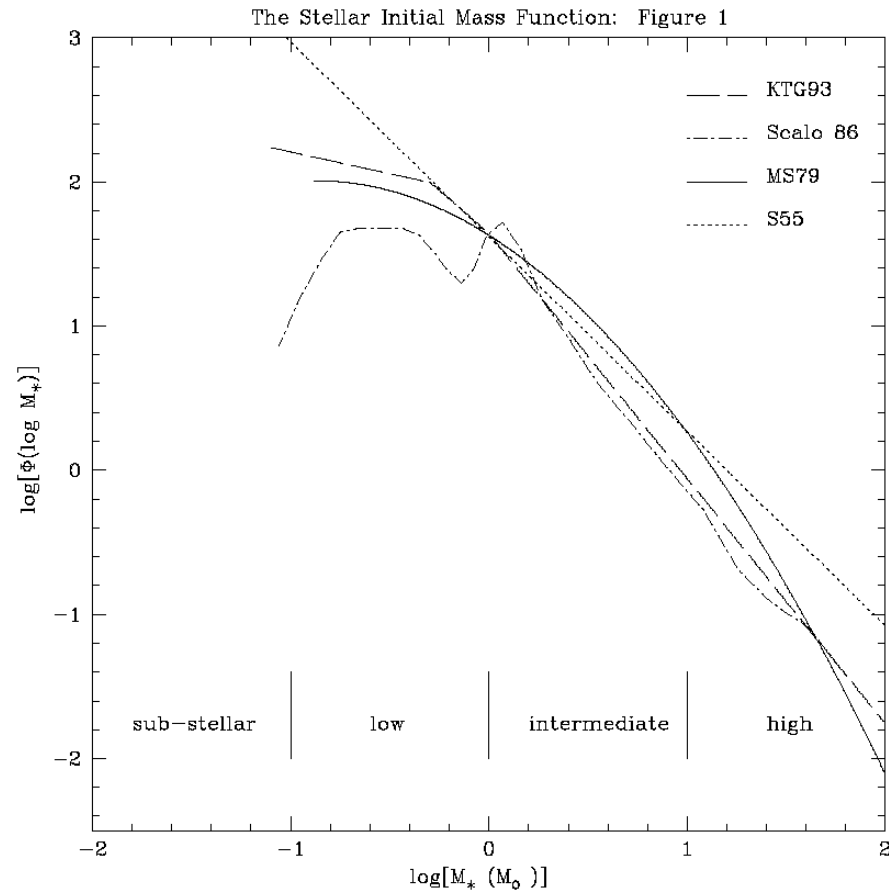
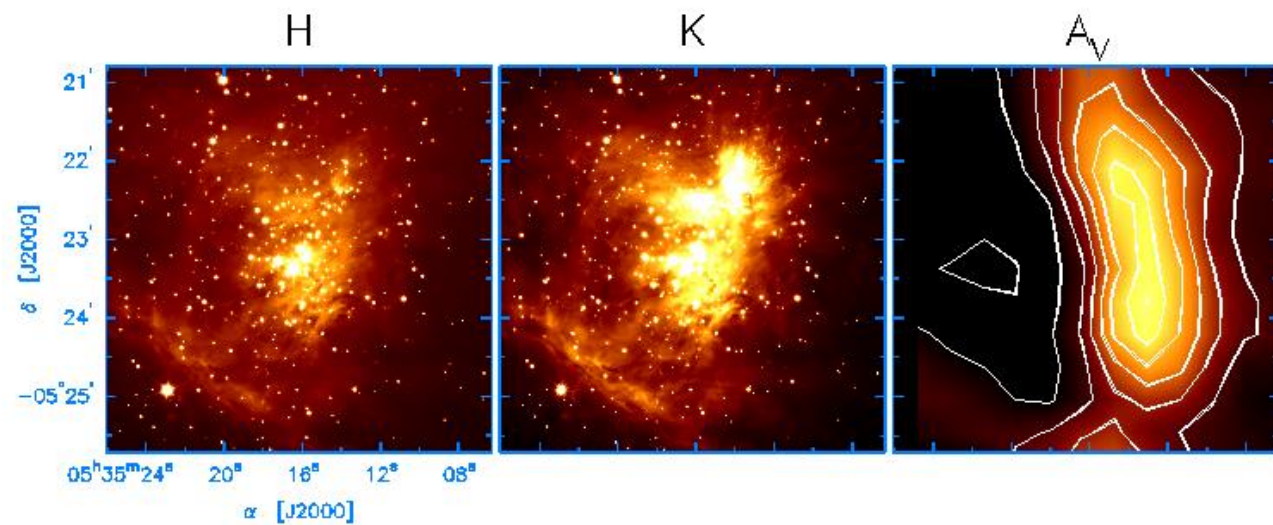


Figure 1. Initial mass function for field stars in the solar neighborhood taken from a variety of recent studies. These results have been normalized at $1 M_\odot$. For both the MS79 and Scalo 86 IMFs we have adopted 15 Gyr as the age of the Milky Way. Current work suggests that the upper end of the IMF ($> 5M_\odot$) is best represented by a power-law similar to Salpeter (1955) while the low mass end ($< 1M_\odot$) is flatter (Kroupa, Tout, and Gilmore 1993). The shape of the IMF from $1-5 M_\odot$ is highly uncertain.

From Meyer et al. (2000) Protostars & Planets IV

Orion Nebula Cluster



<http://www.astro.caltech.edu/~jmc/papers/onc/gif/figure1.gif>

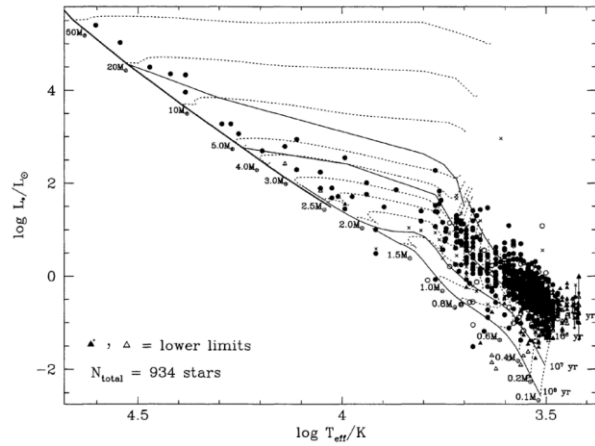


FIG. 12. *HR diagram for the Orion Nebula Cluster.* Triangles indicate lower limits in luminosity. Filled circles/triangles indicate proper motion cluster members plus all sources which have been identified as being externally ionized; open circles/triangles indicate that no proper motion information is available; crosses indicate proper motion nonmembers. Typical errors are ≈ 0.02 in $\log T_{\text{eff}}$ for late-type (K-M) stars but increase towards earlier spectral types, and ≈ 0.2 in $\log(L_*/L_\odot)$ at all spectral types. Two luminosities are plotted for all stars later than M7, with the asterisk indicating the luminosity calculated assuming the star has the $V-I$ color and bolometric correction of an M7 star; see text. Superimposed are the zero-age main sequence and the pre-main sequence evolutionary tracks of D'Antona & Mazzitelli (1994, model 1); over the mass range from $0.1 M_\odot$ to $2.5 M_\odot$; Swenson *et al.* (1994, model F) from $3 M_\odot$ to $5 M_\odot$; and Ezer & Cameron (1967) from $10 M_\odot$ to $50 M_\odot$. The apparent trend of increasing stellar age with mass suggests errors in the zero point of the pre-main-sequence evolutionary tracks, i.e., the initial mass-radius relationship with which the calculations begin.

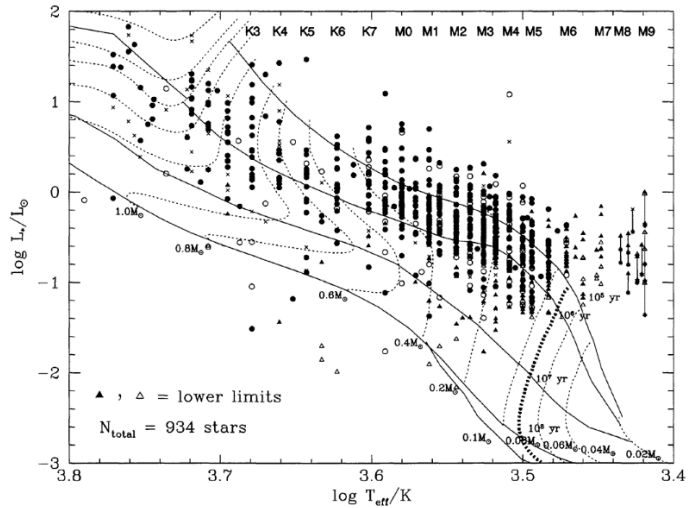


FIG. 13. *Low-mass end of the HR diagram for the Orion Nebula Cluster.* All lines and symbols are the same as in Fig. 12, with the pre-main sequence evolutionary calculations of D'Antona & Mazzitelli now shown down to $0.02 M_\odot$. The hydrogen-burning mass limit of $0.08 M_\odot$ is emphasized. The temperature-spectral-type relationship over the range from K3-M9 is denoted. Note the locations of stars M6.5 and later relative to the tracks. These are probably young brown dwarfs. For a magnitude-limited sample restricted to $I_C < 17.5$ mag, our data begin to become incomplete at ages older than 1 Myr and masses less than $0.1 M_\odot$, assuming a typical extinction of $A_V = 2$ mag.

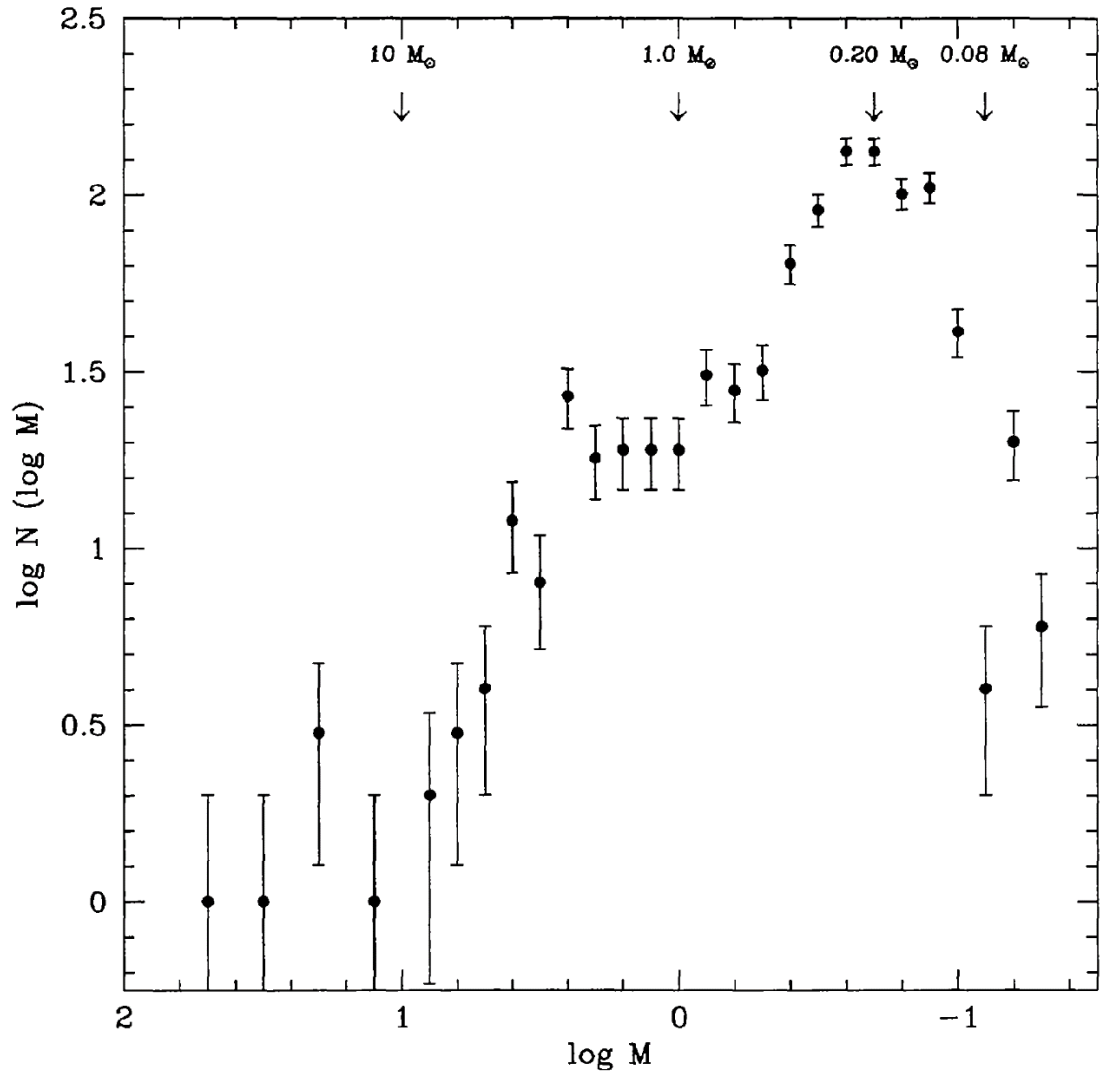


FIG. 17. *The Initial Mass Function as measured in the Orion Nebula Cluster.*

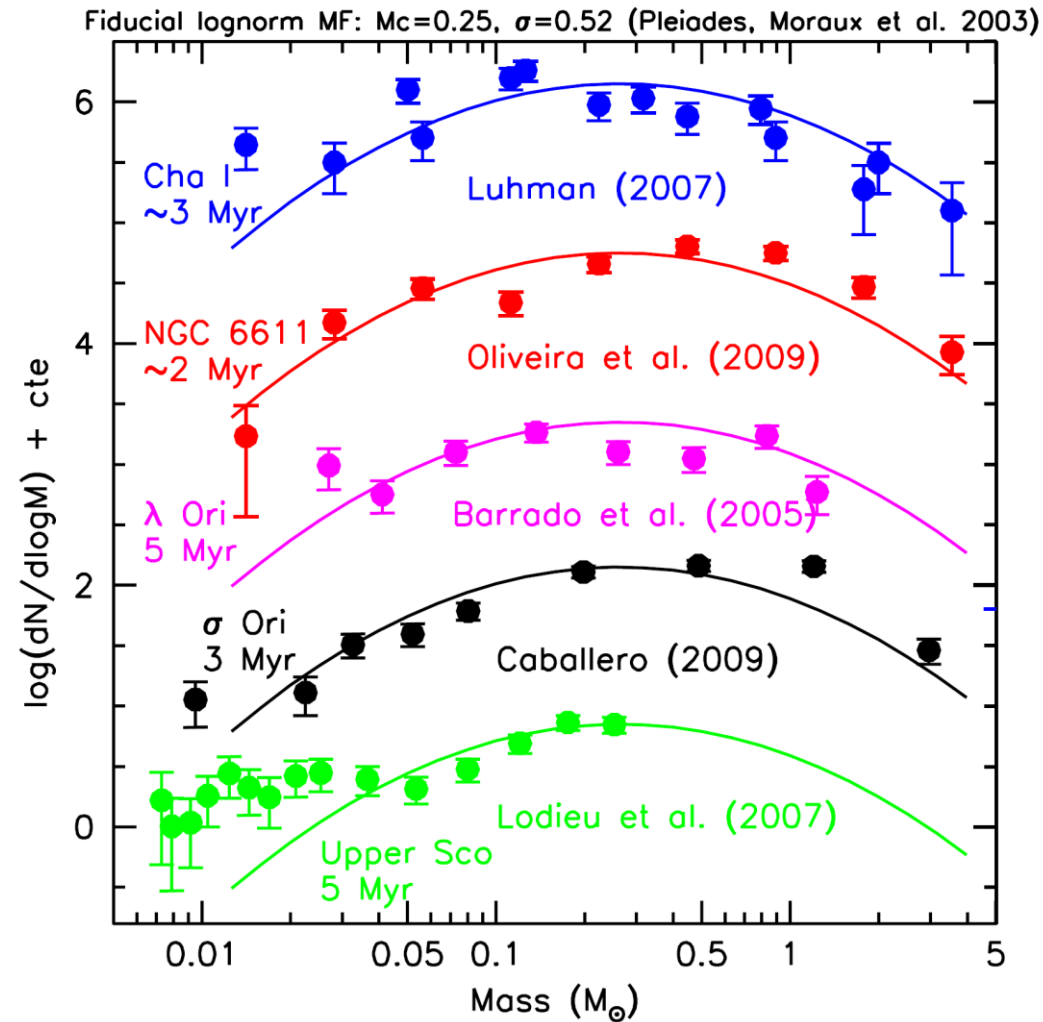


Fig. 9. The IMF determined in a number of young (< 10 Myr) clusters and star forming regions (offset for clarity). The solid lines show the log-normal model that best fits the Pleiades (see Fig. 8). The MFs may be generally consistent with that of the Pleiades but the MF of Upper Sco is quite different. Figure constructed by Bouvier & Moraux.

Stellar Initial Mass Function and Dense Core Mass Function

